NATIONAL ADVISORY COMMITTEE FOR AERONAUTICS

TECHNICAL NOTE 4137

FATIGUE BEHAVIOR OF AIRCRAFT STRUCTURAL BEAMS

By W. S. Hyler, H. G. Popp, D. N. Gideon,
S. A. Gordon, and H. J. Grover

Battelle Memorial Institute

Washington
January 1958

NATIONAL ADVISORY COMMITTEE FOR AERONAUTICS

TECHNICAL NOTE 4137

FATIGUE BEHAVIOR OF AIRCRAFT STRUCTURAL BEAMS

By W. S. Hyler, H. G. Popp, D. N. Gideon,
S. A. Gordon, and H. J. Grover

SUMMARY

This investigation involved a study of the correlation of composite structural fatigue behavior, basic material, and simple-element behavior. Fatigue and related static tests were made on aluminum-alloy box beams and I-beams and also on elements simulating key failure locations in the two beams. The study indicates that the simulation approach will be useful for those cases where it is possible to assess reasonably factors contributing to stress-raisers in the structure. The more complex the secondary stress picture becomes, the more exacting will be the requirements of the stress analysis.

Fatigue notch factors K_f much higher than might be expected from data on simply notched coupons were found in both beams. The study of the simulation elements suggested that such high fatigue notch factors may be expected in composite structures involving stress gradients and biaxial stress distributions at or near rivets. This observation serves to emphasize that considerable caution should be exercised in design in using K_f values obtained from simply notched coupons.

The simulation approach thus appears to provide a technique, in some cases, for evaluating the fatigue strength of composite structures. Use of such simulation elements embodying complex stress influences also appears to be a helpful research tool in determining values of K_f which may be more realistic for designing built-up structures than those which can be obtained by simply notched coupons.

INTRODUCTION

Aircraft structures are often so complex that prediction of their resistance to fatigue cracking is impossible. Available fatigue data on laboratory-test pieces do not reproduce the detailed stress concentrations in the structures and are of limited help in design. At present,

the laboratory data serve chiefly as guides which the designer must use with discretion and, sometimes, with considerable uncertainty.

Several studies of the fatigue performance of actual structures have been reported (see, for example, refs. 1 to 6). In many of these, there is insufficient information on the details of localized stresses in the structure to permit complete analysis with respect to laboratory data on the basic materials involved. In some instances, such analysis as feasible has indicated the fatigue strength of the structure to be significantly less than that estimated from data on simple material coupons. Values of the fatigue notch factor K_f reported for structures have been high in comparison with values for simple coupons having sharp notches. Such observations imply that design, based on laboratory data on simple specimens, may be unconservative.

Accordingly, it seemed interesting to attack this problem from a different point of view. This was to test a composite structure in fatigue and then to attempt to devise simple coupons which, under appropriate loading, would duplicate the mode of failure and the fatigue lifetime of the structure. In other words, the approach was to find what kind of simple coupons would effectively duplicate the stress concentrations in the composite structure.

It was believed that this approach might clarify the apparent gap between observed behavior of structures and laboratory-test data on simply notched specimens. Moreover, if it could be shown that simple specimens can be devised for reasonable duplication of behavior of a composite structure, this should be a useful procedure in some design problems. An aircraft engineer might make a detailed stress analysis of one prototype and/or a fatigue test of one sample of a new structure to determine regions critical in fatigue. Then, simple specimens duplicating the fatigue behavior of these regions could be used for a fatigue-testing program adequate to obtain Goodman diagrams to cover all stress ranges of design interest.

The structures chosen for the investigation were built-up beams of aluminum alloy. One was a box beam, the other, an I-beam. As will be noted subsequently, fatigue failures in the box beam were in the web section. The I-beam structure was designed to produce failure in the chord. It was believed that study of the two types, with different modes of failure, would provide a reasonable investigation of the "simulation element" approach.

During the course of this investigation, valuable suggestions were received from a number of people. The authors would like to express their appreciation for help and suggestions particularly to the following: Messrs. M. Rosche and P. Kuhn, National Advisory Committee for Aeronautics, Mr. R. L. Templin, Aluminum Company of America, and

Mr. S. Levy, General Electric Company. Credit also is due the McDonnell Aircraft Corporation and the Columbus Division of North American Aviation, Inc., for the construction of the beams tested.

This investigation conducted at the Battelle Memorial Institute was sponsored by and carried out with the financial assistance of the NACA.

INVESTIGATION OF BOX BEAM

Design of Box Beam

A number of factors governed the choice and design of suitable structures. It was believed that the structures should be fabricated with material for which considerable basic fatigue data are available. To simulate typical aircraft construction, the structures were built up of extruded angles and sheet materials. Since it was considered necessary to know the actual stresses in the structure, each structure was simple in design. For further simplicity, it was decided to make the structures symmetrical.

For the first structure, these considerations suggested a box-beam specimen subjected to four-point loading. This would provide a constant-stress midspan and would eliminate shear deformation in the test area. The design was such as to make the skin nonbuckling throughout the range of fatigue loading.

Factors chiefly related to accurate stress analyses and to consistency in the location and mode of failure of the beam were considered in the detailed design of the box beam. The following factors were regarded to be of major importance:

(1) A reasonable length of midspan section to insure pure bending (no shear deformation)

(2) Careful design of support and load points to preclude the possibility of failure at supports and in the overhang

(3) Rivet spacing and unsupported skin proportioned to prevent buckling through the expected range of fatigue loading

(4) Use of bare 2024-T3 aluminum-alloy sheet and 2024-T4 aluminum-alloy extrusions to take advantage of the volume of fatigue data available. Brazier-headed rivets were used throughout for the same reason.

Figure 1 is a schematic drawing of the box beam. As noted, the beam was 60 inches between the end supports and the midspan length was

24 inches. Beam depth was 6.128 inches, and the top and bottom skin width was $2\frac{5}{8}$ inches. Two diameters of brazier-headed rivets were used: for the 2017-T3 aluminum alloy, 5/32-inch diameter; for the 2024-T3 aluminum alloy, 3/16-inch diameter. Web stiffeners were of 2024-T4 alloy, 5/8 inch wide and 1 inch deep in cross section; they were spaced 3 inches between centers. Mechanical properties of sheet and chord-angle materials used are listed in table I.

The design of the stiffeners represented the greatest departure from normal aircraft construction of any of the elements in the box beam. This compromise was made to keep construction costs within reasonable limits; it was considered justifiable since the center of the beam contained no shear. The appendix of this report contains a summary of computations of moments of inertia, of interrivet buckling loads and stresses, and of deflections.

Not illustrated in figure 1 is the construction near the load and support points; however, this construction can be inferred from figure 8 which is dicussed later in the report. At these points, solid rectangular blocks of aluminum alloy were used, drilled to permit press-fit assembly of hardened steel bushings. Inside the webs (between web and solid block), 0.051-inch sheets were so designed that the shear load was gradually dissipated in the constant-moment section. This was accomplished within 6 inches of the center line of each support. It was believed that such construction would preclude failures near load and support points.

Loading and Stress Analysis of Box Beam

Figure 2 shows the beam in position on the fatigue-testing machine (used for static loading for stress analysis as well as for repeated loading in fatigue testing). Figure 3 illustrates some details of the fixture for application of load. This fixture was designed to permit free rotation at support and load points. Supports consisted of pins through hardened-steel bushings in the box beams. Ball bearings were pressed on the pins to provide rolling support on hardened and ground blocks. Four loading screws joined the bearing plate to the base plate (attached to the movable head of the fatigue-testing machine). These screws were used for the mean load adjustment. On the reduced section of each loading arm, eight SR-4 strain gages were attached, four on each side of the arm. This arrangement, with calibration, was used for measurement and adjustment of the load.

The fatigue machine used in this investigation has a capacity of 50,000 pounds. The platen movement ranges up to 2 inches, adjustable

with the large cam at the front of the machine (fig. 2). Speed is adjustable up to about 250 cpm; these tests were run at 220 cpm.

It was believed that some of the most important data for comparison of structure and element behavior would be provided by rather complete strain-gage surveys. Furthermore, a detailed strain-gage survey would provide (1) possible evidence of unexpected stress irregularities, (2) possible regions of buckling for loads contemplated in the fatigue-testing program, (3) stress distribution on various cross sections in the midspan, and (4) stress variation along the extreme fibers of the midspan.

Accordingly, the first beam was investigated under static loading prior to the fatigue test. Inside and outside the beam, 78 SR-4 strain gages were attached at critical locations. Load was applied to the loading arms in increments of about 18,000 inch-pounds of bending moment up to a maximum moment of 90,000 inch-pounds. Strain measurements were made at each load level. The results were examined carefully for stress distribution and stress irregularities.

Subsequent tests on other beams contributed additional information on stresses and static behavior. The results of this additional work and of the initial stress analysis are as follows:

(1) At each section investigated, the stress distribution was essentially linear. Figure 4 shows results of a representative section.

(2) At many gage locations, the stress varied linearly with bending moment to a moment of 90,000 inch-pounds. Figure 5 shows this variation for a number of gages located on a section at the midspan. A number of other gages showed some departure from linearity in the stress versus bending-moment plot. The curves in figure 6 are typical of curves prepared from data obtained with these gages.

(3) The middle 12 inches of the midspan were essentially at constant stress. There was no detectable dropoff in outer fiber strain up to 3 inches from the center line and a decrease of only 3 percent at 6 inches either side of the center line. There was a gradual decline in stress toward the load points.

(4) Strain measurements between the vertical row of rivets connecting the web and stiffener indicated secondary tensile stresses transverse to the beam. Figure 6 shows typical results.

(5) No localized buckling was observed up to a compression flange-skin stress of 45.0 ksi (117,000 inch-pounds of bending moment). This compares with a calculated buckling stress of 40.0 ksi. Final collapse occurred 6 inches from the inner load point and in the constant-moment section at about 130,000 inch-pounds of bending moment.

(6) Beam deflection was linear with applied load up to about 99,000 inch-pounds of bending moment.

Fatigue Tests of Box Beams

Two factors governed the choice of fatigue-test conditions: (1) The load factor was to approximate that used in commercial aircraft design, and (2) the alternating loads were to approximate loads that might be experienced by commercial aircraft. A mean stress of 14.0 ksi on the extreme fiber was selected. This corresponds to a 1.0g loading for a load factor of 4.6. Alternating loads ranged from about ±0.30g to about ±0.93g.

Each box beam tested had a number of strain gages attached. These were used to load each beam to its predetermined maximum stress and minimum stress. The strain gages on the calibrated loading arms were used to determine the actual applied bending moments. During each test, the strain behavior was observed at selected intervals.

After the first few fatigue tests, small copper wires were cemented to subsequent beams in the region of expected failures. When a fatigue crack occurred under the wire, the wire broke. The wire was energized so that failure of the wire stopped the machine. This technique permitted the observation of the early stages of crack development. For half of the beams, the test was terminated when the crack or cracks first were observed. In these cases, the box beams were turned over and retested under other stress conditions. With this technique, additional data points were obtained from the limited box-beam specimens available for this work.

Six box beams were tested in fatigue. Three of these were turned over and retested under different stress conditions after the first crack was detected. Some beam tests were carried to complete destruction (complete destruction as defined herein occurred when the crack or cracks progressed at least half the depth of the beam); load-carrying ability of the beam was reduced essentially to zero. For these cases, the number of cycles of stress from initial crack detection to complete failure was never greater than 15 percent of the total lifetime.

Table II presents a summary of specific test information and results for each beam tested. These include bending moments, fatigue life, web stresses deduced from strain measurements, and calculated web stresses (based on gross area and on net area). The measured and calculated stresses were at the line of rivets joining the web and chord angle where failures were initiated.

Stress-lifetime data (stress values based on strain measurements) are plotted on S, log N coordinates in figure 7. An S-N curve is drawn through the plotted points.

Table III summarizes failure data on the six box beams. In this table, the locations of the fatigue cracks are given by component and by numbered rivet hole. Figure 8 should be used in conjunction with this table for identification of the rivet hole. Of the 29 fatigue cracks observed, 25 occurred in the middle 12 inches of the midspan, the constant-stress area (fig. 8). The remaining four cracks were nearer to but not at the load points. In fact, it will be noted generally that fatigue cracks outside the middle 12-inch region were accompanied also by fatigue cracks within the region. With but two exceptions, fatigue cracks were associated with the rivet hole in the web and chord angle at the rivet row common to the chord angle, web, and stiffener. Typical failures in some of the box beams are shown in figures 9 and 10.

Simulation Elements for Box Beam

Possible correlation of the results of the fatigue tests of the box beams with previously reported results of fatigue studies of simple elements (refs. 7, 8, and 9) was investigated. These simple elements (including specimens with a hole, having $K_t = 2$, and specimens with an edge notch, having $K_t = 5$) did not resemble the geometry of critical regions of the beams but were of the same material, 2024-T3 aluminum alloy. It was noted that the shape of the S-N curve for the beam is different from shapes of S-N curves for these elements.

This lack of correlation is not too surprising, since these simple geometric notches are considerably different stress-raisers from those occurring in a complex structure. They do not contain the secondary stiffnesses of a structure, the redundancies of several stress-raisers, or residual stresses and other factors associated with the beam. Accordingly, it was considered desirable to isolate elements from the box beam, to test these in fatigue, and to compare their performance with that of the box beam.

First element.- The first structural element was chosen to duplicate the riveted joint between the web and chord angle. This was the region including all fatigue failures. Figure 11 shows the element details. This specimen was designed to have its gross area centroid coincident with the loading axis. Thus, extraneous bending stresses were minimized.

Each specimen had a number of 1/4-inch SR-4 strain gages attached in the longitudinal direction. The element was loaded to duplicate

essentially the measured strains in the box beam. The mean stress was about 12.5 ksi (based on strain measurements). The data are summarized in table IV and are plotted in figure 12.

It is observed from the table that all failures of the element were one or two rivets removed from the minimum test section. All these failures were in the chord angle. This represents a different mode of failure than was observed in the box beam. The difference between fatigue behavior of this element and of the box beam (fig. 12) probably reflects this difference in the mode of failure. Therefore, no further work was done on this element.

Second element.- It was thought that other factors might be influencing failure of the box beams. In reexamining the beam failures, it was noted that most of the failures were at the rivet holes common to the chord angle, web, and stiffener. It was believed that secondary stress imposed in the web by the stiffener might contribute to failure. One such secondary stress was thought to be a transverse tensile stress between the two rivets which extended through the stiffener. If these rivets filled the holes, the normal transverse shortening of the web (Poisson's effect) due to the longitudinal bending stress would be resisted by the bulky stiffener. This transverse tensile stress was apparent in a static test of a box-beam specimen (see fig. 6). In this study, 1/4-inch SR-4 gages were cemented on the web as close to the chord angle as possible.

The second structural element was designed to incorporate such a secondary stress. Figure 13 shows a diagram of the element. It consists of two stiffener blocks riveted to a sheet of web material. Two 3/16-inch-diameter rivets complete the assembly. It is noted that these rivets are on a line perpendicular to the loading direction. Thus, if they fill the hole, transverse deformation might be inhibited.

Grooves were machined in the stiffener blocks of two specimens for mounting the 1/4-inch strain gages on the sheet between rivet holes under the stiffener blocks. These strain gages were mounted transversely and longitudinally to the loading direction. Two specimens were calibrated statically. As indicated in figure 14, the ratio of the longitudinal stress to the transverse stress of the element was nearly the same as that for the box beam (from fig. 6).

A number of these elements were tested in repeated axial loading. Strain gages were not used on all specimens because of the close approximation in measured stress and calculated stress (gross area). It is believed that the nominal mean stress ranged from about 12.5 ksi to about 13.0 ksi in these tests. These values compare closely with the mean stress values for the box-beam tests (12.1 ksi to 12.9 ksi).

The test results are summarized in table V and are plotted in figure 15. In the figure, the dashed line is the S-N curve for the elements; stresses are calculated from strain-gage readings or are calculated on the basis of gross area. The solid line represents the S-N curve of the box beam. It appears that the two curves coincide with the probable precision of either test.

INVESTIGATION OF I-BEAM

Design of I-Beam

After experience in the box-beam investigation, it was decided to study a fabricated I-beam of somewhat greater length and depth than those of the box beam.

It was thought that this type of beam would afford a good chance of a fatigue failure in the chord which would be a different mode of failure than that obtained in the box beam. Simplicity of design suggested that the I-beam be loaded in a manner similar to that used in the box beams.

To insure, as much as possible, that fatigue failures would occur in the chord section, the following precautions were taken:

(1) Chord cross-sectional area was reduced in the outer flange of the beam at the midspan center section.

(2) Rivet holes in the web section around the critical span (center 8 inches) were reamed and deburred.

(3) Outer edges of the web were broken with fine-grit paper.

(4) The edge distance for the rivet row was made greater in the web than in the chord.

Schematic drawings of the I-beam are shown in figures 16 and 17. The principal dimensions for the I-beam are shown in these drawings. As noted, in the center 8 inches of the midspan the depth of the beam was reduced to $9\frac{3}{4}$ inches for reasons discussed previously.

The materials used for the various parts of the structures were as follows: For web, spacers, and shear plates, 0.072-inch 2024-T3 aluminum-alloy bare sheet; for chords and stiffeners, 2024-T4 aluminum-alloy extrusions; for bushing housings, 2024-T4 aluminum-alloy plate; and for

the 3/16-inch-diameter Brazier headed rivets, 2024-T3 aluminum alloy. The mechanical properties of these materials are shown in table VI.

As indicated in figure 17, the moment of inertia of the center section of the beam based on net-area calculations was $I_{xx} = 40.88$ inches^4. The moment of inertia based on gross areas I_{gg} was 41.55 inches^4. Typical computations of moment of inertia and of deflection are shown in the appendix.

The construction of the beam near the support and load points is illustrated in figure 18. At these points, construction is similar to that used on the box beam. However, the solid rectangular blocks of aluminum are on the outside of the beam. On each side of the web and extending over the chords are shear plates, which gradually dissipate the shear load into the constant-moment section.

Loading and Stress Analysis of I-Beams

The loading fixture for testing the I-beams was essentially the same as the one used in testing the box beams. The main difference was that the fixture was larger to accommodate the larger beam. Load was applied through calibrated loading arms equipped with strain gages. The fatigue-testing machine and the machine speed were the same as those used for the box-beam tests.

As in the box-beam tests, a thorough static-stress calibration of the I-beam was considered necessary prior to the fatigue test.

Accordingly, the first of the beams to be tested in fatigue was statically calibrated. A number of strain gages were cemented to the beam. The load was applied in increments of 45,000 inch-pounds of bending moment in the midspan to a maximum moment of 270,000 inch-pounds. A bending moment of 270,000 inch-pounds corresponds to a stress of 30 ksi in the outer fibers at a section through the midspan center line of the beam. Strain measurements were taken at each load level. The results were examined carefully for stress distribution and stress irregularities.

During the course of the fatigue tests, additional experimental stress studies were made to provide other information as it appeared necessary. For example, after completing fatigue tests on the first beam, it was decided to remove the center stiffeners (marked A in fig. 18) on the second beam prior to testing. A stress study was made in selected regions of the second beam before and after the stiffeners were removed. The results of all stress analyses are as follow:

(1) In the reduced section of the beam, the stress distribution with depth was almost linear. Figure 19 shows a representative section. An exception to this was observed on a section at the edge of the fillet machined on the chord.

(2) At sections outside the reduced section of the beam, the stress distributions were not linear. For example, at section B-B (about 6 inches from the midspan center) there was almost a constant stress across the chord, whereas web stress distribution was linear. A nonlinear distribution was also found on a section through the first rivet in the shear plate (see fig. 20; note the slight variations in stress distribution on this section for the individual beams).

(3) At all gage locations, the principal stress varied linearly with applied bending moment. For any one value of applied bending moment, there was a gradual reduction in stress with distance from the midspan center line of the beam.

(4) An exception to item (3) was noted on the outer fibers of the tension and compression flanges. At these regions, a peak stress occurred 4 inches from the midspan center line. This position is coincident with the fillet. The peak stress at these points was about 20 percent higher than was the stress at the midspan center line of the beam on these surfaces.

(5) Secondary stresses perpendicular to the midspan direction were greatest in the web in an area around the stiffeners and the first rivet in the shear plate. These stresses were, with the stiffeners in place, less than 1 ksi of tensile stress and, with the stiffeners removed, less than 2 ksi of compressive stress. The measured principal stresses were not affected appreciably by the removal of the center stiffeners.

(6) With the stiffeners in place, no buckling was observed through the stress range investigated. A small amount of buckling was observed in the web when the stiffeners were removed. However, this was not considered sufficient to affect the fatigue results.

(7) Beam deflection was linear with applied load up to 270,000 inch-pounds of bending moment. The magnitude of the measured deflection compared closely with the magnitude of the calculated values for deflection (see calculations in appendix).

Comparison of the results of the experimental stress analysis with the results of the theoretical analysis showed the beam to be behaving about as had been anticipated.

Fatigue Tests of I-Beams

The fatigue tests on the I-beams were run under loading conditions analogous to those for the box beam. The loads approximated those used in commercial aircraft design. All beams were tested at a mean stress of 14 ksi of the extreme fiber of the midspan center section. This stress is equivalent to 1.0g loading based on a load factor of 4.5. Alternating load varied from ±0.49g to ±0.93g.

The strain gages attached to each beam served (in loading the beam) to determine maximum and minimum stresses. The strain gages on the loading arms were used to balance the load and to measure the applied bending moment. Throughout the test, a number of load and strain readings were taken to correct for load changes during the test. Crack-detection wires also were used to determine occurrence of the first crack, thus preventing catastrophic failure of the beams. When the first crack was detected, the test was considered complete. The beam then was turned over for a second test.

Two I-beams were tested in fatigue. By using the technique described above, four sides of the beams were tested and four points on the S-N curve were obtained.

Table VII summarizes the fatigue-test results. The table indicates which member of the structure failed and the crack location by the use of numbered rivets. These numbers correlate with numbered rivets in figure 18.

In all, there were seven fatigue cracks detected. All but one of these were in the chords. The one crack in the web was located at a rivet at which failure in the chord also was detected. This failure was in the fourth beam side (specimen 2-1) tested. Of the six failures remaining, five were located in the chord at a common rivet hole associated with the first rivet in the shear plate, $8\frac{3}{4}$ inches from the center of the beam. Of the three beam sides failing at this location, two had failures in both chords at this rivet hole. The remaining failure, that in the first beam (specimen 1), was in the reduced section of the chord. However, it was associated with a metallographic flaw in the surface of the extrusion. Therefore, this test was not considered characteristic of the beam. A typical I-beam failure may be seen in figure 21.

Table VIII presents the stress data for I-beams. In the table are indicated the bending moment applied to the midspan, the stresses at the point of failure as determined from the static calibrations, the lifetime in cycles to crack detection, and the calculated stresses (based on both net effective area and gross area).

Stress-lifetime data for the three beam sides for which failure occurred at the edge of the rivet hole in the chord are plotted on S, log N coordinates in figure 22. Stresses are based on strain measurements obtained in the vicinity of failure, extrapolated to the failure location (see section entitled "Elements Constructed From Beam Material").

Simulation Elements for I-Beam

The I-beam had been planned to fail in fatigue in the chord at a section where the stresses could be analyzed relatively easily. While the beams failed in the chord angle, failures initiated at a region of considerable complexity for detailed stress analysis. However, it was decided to proceed, with the somewhat limited information available concerning local stresses in the I-beams at this location, in construction of simple elements which might duplicate the fatigue behavior observed.

Comparison of the S-N curve for the I-beam with curves for simply notched specimens (refs. 7, 8, and 9) and with curves for the two types of element for simulation of behavior of the box beam showed dissimilarities. Accordingly, consideration was given to design of a different type of element.

Preliminary experiments.- Failures in the I-beam were in the extruded chord angle at a rivet hole which contained the last rivet in the shear plate. At this location, a number of factors contributed to the local stress distribution. These included (1) the discontinuity in the structure at the termination of the shear plate, (2) the secondary stresses in the chord angle from the shear plate, (3) the stress concentration of the filled rivet hole, and (4) the residual stress from fabrication.

Three types of elements intended to contain similar factors were fabricated from available 0.081-inch 2024-T3 sheet stock (to conserve the small remaining supply of actual materials used for the I-beams). Figure 23 shows the specimen designs. In these specimens the main sheet is considered to represent the chord angle of the beam; the side plate or plates which end just short of the transverse center line of the specimen are considered the shear plates. As shown in figure 23, each end of the specimens contained six rivets in a line.

Three specimens of type A were tested at nominal (P/A) stresses of 8.0 ± 6.0 ksi. These failed in lifetimes from 300,000 to 600,000 cycles. However, failure initiated under the "shear plate" in the "chord angle" at regions of intense fretting. This was ascribed to local stresses resulting from nonsymmetry in the thickness direction.

A specimen of type B (planned to reduce the nonsymmetry) was next tested. This lasted, under the same nominal stress range in the chord sheet, more than 3,000,000 cycles. However, eventual failure was again near the edge of the shear plate and fretting was again present.

One condition in the region of failure of the I-beam, not duplicated in these elements, was a stress gradient. Accordingly, two specimens of type C were constructed and tested. In these, the line of loading was slightly (about 1/4 inch) offset from the line of rivets. Strain gages on these specimens were used to (1) verify that a strain gradient existed across the width and (2) obtain, by extrapolation, values of the strain in the chord sheet at the position of the last rivet in the shear plate. The following results were obtained (see footnote of table IX for method of computing stresses):

Specimen number	Nominal stresses in sheet at rivet		Lifetime, cycles
	From computations	From strain gages	
1	10.4 ± 7.7	7.0 ± 5.3	608,000
2	16.8 ± 10.7	8.3 ± 6.1	146,000

For both specimens, failure occurred at the edge of the rivet hole corresponding to the last rivet in the shear plate. Thus, the mode of failure was similar to that in the I-beam. Since the lifetime for the elements, for stress conditions roughly similar to those in the I-beam, were in the range of the beam lifetimes, it seemed reasonable to carry out further studies with this type of specimen.

Elements constructed from beam material.- Accordingly, seven elements similar to those of type C (fig. 23) were machined from materials used for the I-beams. Figure 24 shows the dimensions and configuration of the center section of this (type D) specimen. The sheet was the 0.072-inch material from stock used on the I-beams. The chord sections were planed to 0.072-inch thickness from the extruded-angle stock used for the I-beams.

Some 32 strain gages were used on each specimen. A number of these served mainly to assist in loading for reasonable symmetry (for example, to minimize bending) and to assist in estimating the overall strain pattern. The locations of the eight gages generally used for loading and evaluations of stresses are shown in figure 24.

The loading procedure was as follows (see fig. 24). Stresses were extrapolated linearly from gages 1 and 2 to position X at the rivet where failure was expected. Similar extrapolations were made from

gages 3 and 4 and from gages 5 and 6 and 7 and 8 to the corresponding position Y. After reasonable adjustment (by shims, etc.) to provide minimum bending and twisting, the average of these extrapolated values on the higher stress end was used for a loading stress. Table IX shows these stresses and the observed lifetimes to failure. Figure 25 shows the results on an S-N plot (loading stresses used for plotting).

A dashed line is drawn through the points representing data for the elements. It will be noted that two of the data points fall much below this line. Evidence from additional strain gages indicated that the corresponding two specimens had strain distributions (particularly across the chord sheet between the shear plates) which was extreme in comparison with those of the other five specimens. It is possible that these underwent twisting in adjustment of the grips, but the only certain conclusion is that they were different in stress distribution. Accordingly, these points were disregarded in drawing the line.

The solid line representing the I-beam is about 20 percent lower than the dashed line. A number of factors which might account for this were considered. The ratio of chord material to shear-plate material was much higher in the I-beam than in the elements. In the I-beam, bending moments provided a different means of transfer of load between chord and shear plate than was present in the element under axial loading. Consequently, the stresses obtained by extrapolation in both cases were really not directly comparable. A limited strain-gage exploration of one specimen (of type D) showed that strain gages on the shear plate had somewhat lower readings than values obtained from linear extrapolation of gages on the edge of the chord of the element. In fact, if the stress amplitude values for the dashed line in figure 25 are reduced by about the value suggested by this experiment (15 percent), the dashed line comes (within the experimental error) in coincidence with the solid line representing the beam.

Justification for the assumption that stresses in the chord underneath the shear plate are equal to those in the shear plate is questionable. The measurements serve to emphasize the difficulties that might attend the simulation-element approach for those complex structures for which fatigue failure might occur in regions where stresses cannot readily be determined.

The type D elements failed in the chord at the edge of the last rivet hole in the shear plate. Thus, the failure mode was the same as that of the I-beam. With reasonable allowance for the manner in which values from strain-gage readings were extrapolated, it appears that the element showed qualitative agreement with the I-beam. However, unlike the box beam it is doubtful whether quantitative agreement could be expected without additional evidence both on simulation elements and on

the I-beam regarding the local strain or stress distribution in the web at or near the chord angle.

DISCUSSION OF RESULTS

Correlation of Fatigue Behavior of Elements With Fatigue Behavior of Box Beam and I-Beam

The simulation approach to studying the fatigue behavior of a complex structure appears to involve a process of duplicating in the simulating elements the stress concentrations in the composite structure. Once it is shown that simple elements can provide a reasonable duplication of the behavior of a composite structure it may be possible to use such elements to establish Goodman diagrams for the range of stresses of design interest. This latter idea, of course, also will need verification. As indicated subsequently, the use of such elements, embodying the secondary stresses and stiffnesses found in actual structures, as a research tool in fatigue studies also may provide more realistic values of K_f pertinent to aircraft structures than can be obtained by simply notched coupons or lap-joint specimens that have been examined in the past.

In this investigation the simulation approach was studied for two built-up structures - a box beam and an I-beam. In the former case (the box beam) failures initiated in the web at rivets joining the web and chord angle (passing through the solid stiffener). In this area, longitudinal stresses were present and also transverse tensile stresses; the latter were presumed to be imposed by the block stiffener preventing the normal transverse shortening of the beam.

Of the two simulation elements studied for the box beam, one contained, in addition to the longitudinal tensile stress, a transverse tensile stress of the order of magnitude of that in the web of the box beam. This element was successful in duplicating the fatigue strength of the box beam. The element not containing the secondary stress was not useful in this regard.

The I-beam was designed to produce failure in the chord angle, a mode of failure different from that of the box beam. Failures of the I-beam did occur in the chord angle but at a location remote from the test section. Specifically, failures initiated at a rivet hole in the chord angle which was the last rivet hole in the shear plate. At this location, a complex condition exists as a result of the discontinuity of the end of the shear plate (which introduces shear and bending

stresses into the chord angle) and of the fretting corrosion of the chord angle under the shear plate.

Three elements were studied in investigating simulation of the I-beam fatigue behavior. Only when secondary bending was introduced into one of the elements was it possible to duplicate the mode of failure (type D). With this element qualitative agreement with the I-beam was achieved within the limitations of the approximations used in extrapolating strain data to the critical section. Quantitative duplication would depend upon an accurate determination of the local stresses both in the I-beam and in simulating elements.

Stress Concentration Factors of Beams

It is common practice, in designing to prevent fatigue, to evaluate nominal stresses and to apply factors to allow for the indeterminable stress concentrations that are so important in determining the initiation of a fatigue crack. One factor often used in such design is the fatigue notch factor K_f. This may be defined by

$$K_f = \frac{\text{Stress amplitude for unnotched material}}{\text{Nominal stress amplitude for part at same nominal mean stress and same lifetime}}$$

It is interesting to consider results of the beam tests in these terms.

Figure 26 shows values of K_f for the box beam and for the I-beam in terms of cycles to failure. These were determined by dividing values of nominal stress amplitude[1] (from tables II and VIII) into values of stress amplitude for unnotched 2024-T3 sheet at a mean stress of 10 ksi (from ref. 7). Since, over this lifetime range, the fatigue strength generally is not highly sensitive to mean stress, no allowance was made for the actual variations in mean stress for the two beams (box beam, 12.1 to 12.9 ksi, I-beam, 7.8 to 8.2 ksi). For comparison, dashed lines in figure 26 show values of K_f for specimens with simple geometrical notches of two severities (taken from refs. 8 and 9).

In the region of higher stresses which produce cracking in about 10,000 cycles, the box beam shows a value of K_f lower than that of a sharp ($K_t = 5.0$) notch in sheet specimens. For lower stress amplitudes corresponding to failure in about 1,000,000 cycles, the box beam shows a much higher value of K_f (of the order of 6.0). The notched sheet shows a decrease in K_f in this range. The I-beam curve (based on only

[1]Maximum stress minus mean stress.

3 points) indicates a trend similar to that of the box beam for K_f. Thus, K_f continues to increase with decreasing stress amplitude. The value of K_f in this case approaches 5.

Similar high values of K_f can be computed from results of other tests on composite structures. Failures at riveted shear joints in C-46 wing tests (ref. 5) provide values in the range of 3.7 to 4.5 at lifetimes of the order of 200,000 cycles; in the same tests, failures at corner inspection cutouts indicate K_f values from 4.8 to 5.3 at lifetimes of the order of 300,000 cycles.

Such observations imply that, in design, it is not safe to apply, to conventional nominal stress values, values of K_f as low as those observed in laboratory tests of even sharply notched coupons.

Factors Influencing Values of Stress Concentrations

The studies of simulation elements for the two types of beams provide some indication of the factors influencing K_f values of structures.

Figure 27 shows values of K_f for (1) the first simulation element for the box beam, (2) a geometric notch ($K_t = 5.0$) in sheet material, (3) the second simulation element for the box beam, and (4) the element for the I-beam. It is obvious that the K_f values for all the simulation elements increase in magnitude for longer values of lifetime (and lower values of nominal stress) than do values of K_f for the geometric notch. It seems possible that these relatively high stress concentrations are related to the complex flow of stress through a rivet as well as the interactions imposed on the components by adjacent rivet geometry. Fretting around the rivet even at low nominal stresses also is a contributing factor.

It is further apparent that the values of K_f are much larger for the second element for the box beam than for the first element. It will be recalled that one difference between the stress distributions in these two elements is the presence of a significant transverse stress in the second element. It may also be recalled that only when there was a stress gradient introduced across the simulation element for the I-beam were failures obtained at the rivet. These observations imply that the effective stress concentration at a rivet can be particularly high in the presence of a stress gradient and of transverse stress.

Simulation Approach

This investigation has demonstrated the feasibility of using simple elements to study the fatigue behavior of complex structures; however, the study also has suggested certain limitations to such an approach.

The main thesis appears to be that simulation can be achieved if it is possible to analyze the structure so well that the stress discontinuities of the structure can be reasonably well duplicated in the simulating elements. For those cases where it may be impossible to characterize the entire nature of the stress irregularities (or their contributory causes) it appears that the simulating element will be less useful.

It would appear that the use of simulation elements can be considered from a somewhat different approach. For example, considerable data have been assembled on simply notched bars and on simple elements, such as riveted lap joints. Such data may be of interest in characterizing the fatigue strength of materials but may be less useful in providing data of general significance in designing complex structures. The specific reason for this is that such notched coupons and simple elements do not contain, in general, the secondary stresses and restraints found in a complex structure and, hence, fatigue notch factors obtained from such specimens may not approach the high values of K_f found in structures. On the other hand, the use of simulating elements which contain stress features found in complex structures should provide more realistic estimates of K_f, which would be of more immediate and useful interest in designing structures to resist failure by fatigue.

CONCLUDING REMARKS

This investigation was initiated to explore the problem of correlating composite-structure fatigue behavior and basic material or simple-element behavior. To this end, fatigue and related static tests were carried out on box beams and on I-beams and also on elements simulating key locations in the two types of beams. Load and stress conditions for the fatigue tests were selected in the range experienced by commercial aircraft.

The following conclusions appear warranted on the basis of the investigation:

For the box beam, the fatigue behavior at the critical location of failure was apparently correlated with the behavior of a simple simulation element. Correlation was obtained when the mode of failure and the secondary stresses were duplicated. For the I-beam there appeared to be

qualitative agreement with a simulation element. Uncertainties in the detailed stress distribution in the region of failure of the I-beam made selection of an element containing the stress irregularities difficult. It thus appears that the simulation approach will be useful for those cases where, by experimental study, it will be possible to assess reasonably factors contributing to stress-raisers in the structure.

High fatigue notch factors (in terms of the conventional definition of stress) were found in both beams. This observation suggests that in design the use of K_f values obtained from simply notched coupons may be an unconservative practice.

The study of simulation elements suggested that such high fatigue notch factors may be expected in composite structures where biaxial stress distributions and marked stress gradients occur around rivets. The importance of riveted construction in aircraft design suggests that further assessment of the effect of complex loadings on the fatigue notch factors of riveted components should be made. If simulation elements are designed to contain typical secondary stress and load influences as observed in structures, the resultant data may yield more useful K_f values than those currently obtained on simply notched coupons.

Battelle Memorial Institute,
Columbus, Ohio, September 30, 1956.

APPENDIX

TYPICAL CALCULATIONS OF MOMENTS OF INERTIA, BUCKLING STRESSES, BENDING MOMENTS, AND DEFLECTIONS

Symbols

The following symbols are employed in this appendix:

A	cross-sectional area of each component of beam, $in.^2$
a	distance between load and support points, in.
b	distance between rivet rows, in.
c	distance to outer fibers, in.
d	distance from centroid of component to respective axis of inertia, in.
E	Young's modulus
I_o	moment of inertia of each component of beam about its own centroidal axis, $in.^4$
I_{gg}	moment of inertia about neutral axis of beam section (gross area), $in.^4$
I_{xx}	moment of inertia about neutral axis of beam section (net area), $in.^4$
K	end restraint constant
l	distance between load points, in.
P	applied load in each loading arm, lb
S	buckling stress, ksi
t	web or flange thickness, in.
v	Poisson's ratio
$\bar{x}$	centroidal distance of net-area section from axis A-A (axis coincident with compression surface), in.

y_1 midspan deflection, in.

y_2 overhang deflection, in.

Summary of Moments of Inertia, Buckling Stresses, Bending Moments, and Deflections of Box Beam

The moments of inertia, buckling stresses, bending moments, and deflections of the box beam are as follow:

Moment of inertia:

Net effective area, inches^4

$$I_{xx} = \sum Ad^2 + \sum I_o - A\bar{x}^2 = 7.75$$

Gross area, inches^4

$$I_{gg} = \sum Ad^2 + \sum I_o = 8.727$$

Flange-skin interrivet buckling stress, ksi:

$$S = \frac{K\pi^2 E t^2}{12(1 - \nu^2)b} = 40.0$$

Flange-skin interrivet buckling bending moment:

Net effective area, inch-pound

$$Pa = \frac{SI_{xx}}{c} = 93,500$$

Gross area, inch-pound

$$Pa = \frac{SI_{xx}}{c} = 113,200$$

Deflection:

Net effective area, inch

$$y_1 = \frac{Pal^2}{8EI_{xx}} = 0.00000088\ Pa$$

$$y_2 = \frac{Pa^2(3l + 2a)}{6EI_{xx}} = 0.0000039\ Pa$$

Gross area, inch

$$y_1 = \frac{Pal^2}{8EI_{gg}} = 0.00000078\ Pa$$

$$y_2 = \frac{Pa^2(3l + 2a)}{6EI_{gg}} = 0.0000035\ Pa$$

Moment of inertia at center of beam:

Net effective area, inches^4

$$I_{xx} = \sum Ad^2 + \sum I_o - A\bar{x}^2 = 40.88$$

Gross area, inches^4

$$I_{gg} = \sum Ad^2 + \sum I_o = 41.55$$

Moment of inertia at section through the first rivet and shear plate:

Net effective area, inches^4

$$I_{xx} = 57.8$$

Gross area, inches^4

$$I_{gg} = 58.67$$

Deflection:

Net effective area, inch

$$y_1 = \frac{Pal^2}{8EI_{xx}} = 0.000000333\ Pa$$

$$y_2 = \frac{Pa^2(3l + 2a)}{6EI_{xx}} = 0.00000156\ Pa$$

Gross area, inch

$$y_1 = \frac{Pal^2}{8EI_{gg}} = 0.000000328\ Pa$$

$$y_2 = \frac{Pa^2(3l + 2a)}{6EI_{gg}} = 0.00000154\ Pa$$

REFERENCES

1. Brueggeman, W. C., Krupen, P., and Roop, F. C.: Axial Fatigue Tests of 10 Airplane Wing-Beam Specimens by the Resonance Method. NACA TN 959, 1944.

2. Anon.: Flexural Fatigue Tests of Some Aluminum Alloy Wing Beams of Several Designs. Prog. Rep. No. 1, Bur. Aero., Aug. 1947.

3. Howard, Darnley M.: Flexural Fatigue Tests of Wing Beams. NBS Rep. 1350, Bur. Aero., Dec. 1951.

4. Johnstone, W. W., Patching, C. A., and Payne, A. O.: An Experimental Determination of the Fatigue Strength of CA-12 "Boomerang" Wings. Rep. SM 160, Aero. Res. Labs. (Melbourne), Sept. 1950.

5. McGuigan, M. James, Jr.: Interim Report on a Fatigue Investigation of a Full-Scale Transport Aircraft Wing Structure. NACA TN 2920, 1953.

6. Howard, Darnley M., and Katz, Silas: Repeated Load Tests of Aircraft Wing Beam Specimens Under Bending and Bending-Torsion Loads. Nat. Bur. Standards Rep. 4720, Bur. Aero., June 1956.

7. Grover, H. J., Bishop, S. M., and Jackson, L. R.: Fatigue Strengths of Aircraft Materials. Axial-Load Fatigue Tests on Unnotched Sheet Specimens of 24S-T3 and 75S-T6 Aluminum Alloys and of SAE 4130 Steel. NACA TN 2324, 1951.

8. Grover, H. J., Bishop, S. M., and Jackson, L. R.: Fatigue Strengths of Aircraft Materials. Axial-Load Fatigue Tests on Notched Sheet Specimens of 24S-T3 and 75S-T6 Aluminum Alloys and of SAE 4130 Steel With Stress-Concentration Factors of 2.0 and 4.0. NACA TN 2389, 1951.

9. Grover, H. J., Bishop, S. M., and Jackson, L. R.: Fatigue Strengths of Aircraft Materials. Axial-Load Fatigue Tests on Notched Sheet Specimens of 24S-T3 and 75S-T6 Aluminum Alloys and of SAE 4130 Steel With Stress-Concentration Factor of 5.0. NACA TN 2390, 1951.

TABLE I

MECHANICAL PROPERTIES[a] OF MATERIALS USED IN BOX BEAM

Material	Tensile strength, ksi	Yield strength (0.2 percent offset), ksi	Elongation in 2 in., percent	Modulus of elasticity, psi
0.064-inch 2024-T3 aluminum-alloy sheet	72.3	53.4	18.2	10.6×10^6
0.051-inch 2024-T3 aluminum-alloy sheet	71.1	52.4	19.2	10.6
3/4- x 3/4- x 0.091-inch 2024-T4 aluminum-alloy extruded angle	67.1	53.2	17.2	10.6

[a]Average strength values from four specimens.

TABLE II

STRESSES IN BOX BEAMS

Specimen	Bending moment Pa, 1,000 in-lb		Fatigue life, cycles	Measured web stress, ksi		Calculated web stress, ksi			
						Based on gross area		Based on net area	
	Maximum	Mean	(a)	Maximum	Mean	Maximum	Mean	Maximum	Mean
1	64.8	41.8	289,850	20.2	12.7	19.4	12.6	23.9	15.4
2	69.8	44.8	193,760	20.6	12.9	20.9	13.4	25.7	16.2
3	82.1	42.8	36,670	24.2	12.5	24.6	12.9	30.3	15.8
4	62.2	42.5	265,380	17.7	12.1	18.7	12.8	22.9	15.6
4-1	56.2	43.7	624,700	15.8	12.4	16.8	13.2	20.7	16.1
5	57.0	44.4	1,137,120	16.7	12.2	17.1	13.4	21.0	16.4
5-1	82.7	43.6	30,540	24.2	12.3	24.8	13.1	31.1	16.4
6	51.2	41.9	5,294,630	15.6	12.7	15.4	12.4	18.9	15.5
6-1	67.1	41.0	108,000	20.3	12.7	20.1	12.3	24.7	15.1

[a]See table III and figure 8 for location of failure.

TABLE III

SUMMARY OF BOX-BEAM FATIGUE FAILURE DATA

Specimen	Data on first observed fatigue cracks				Final failure	Remarks
	Member	Figure illustrating crack	Rivet hole (a)	Fatigue life, cycles	Fatigue life, cycles	
1	Web		2; 5	289,850	289,850	Fatigue-crack detection wire was not used
	Flange		9	289,850		
2	Web	9	2; 5; 5; 5	193,760	193,900	Fatigue-crack detection wire was cemented to flange tension skin only; web appeared to fail at rivet 5
	Chord angle		2; 5; 5; 8	193,760		
3	Web		2; 5; 5; 7	36,670	43,300	Web failed first at rivet 7
	Chord angle		5; 8	36,670		
4	Web		2; 5; 5; 8	265,380		Test stopped; beam turned over for test 4-1
	Chord angle		5	265,380		
4-1	Web		5	624,700	686,530	Web failed first
	Chord angle		5	656,880		
5	Web		2	1,137,120		Test stopped; beam turned over for test 5-1
5-1	Web		5	30,540	32,910	
	Chord angle		5			
6						Did not fail; beam turned over for test 6-1
6-1	Web	10	2	108,000		Test was not continued to ultimate failure
	Flange		2			

[a]See figure 8.

TABLE IV

SUMMARY OF FATIGUE-TEST DATA ON FIRST SIMULATION ELEMENT FOR BOX BEAM

Specimen	Fatigue life, cycles	Measured stress, ksi		Calculated stress, ksi				Location of failure
				Based on gross area		Based on net area		
		Maximum	Mean	Maximum	Mean	Maximum	Mean	
1	533,000	19.5	12.6	21.1	14.1	24.9	16.6	Angle; $1\frac{3}{4}$ in. off center
2	767,000	19.0	12.2	20.3	14.5	23.9	15.4	Angle; 7/8 in. off center
3	428,000	21.3	11.2	21.8	11.7	25.6	13.8	Angle; $1\frac{3}{4}$ in. off center
4	165,000	25.4	12.8	25.1	12.8	29.5	15.0	Angle; $1\frac{3}{4}$ in. off center
5	791,000	17.9	12.0	18.8	12.8	22.1	15.1	Angle; $1\frac{3}{4}$ in. off center
6	16,625,000	17.4	14.0	16.2	12.8	19.0	15.0	Did not fail
[a]6-1	9,634,000	----	----	17.9	12.8	21.0	15.0	Angle; 7/8 in. off center

[a]Retest of specimen 6.

TABLE V

RESULTS OF FATIGUE TESTS OF SECOND SIMULATION ELEMENT FOR BOX BEAM

Specimen	Fatigue life, cycles	Calculated stress based on gross area, ksi (a)	Calculated stress based on net area, ksi (b)	Location of failure
7	35,700	25.0	33.5	Center
8	92,900	21.0	28.1	Center
9	278,400	18.0	24.3	Center
10	432,000	17.0	22.8	Center
11	2,787,000	16.0	21.4	Center
12	47,000	23.0	30.8	Center
13	1,244,000	16.5	22.1	Center
14	289,000	19.0	25.2	Center
15	+20,019,000	15.5	20.8	Did not fail
16	2,446,600	16.0	21.3	Center
17	+25,165,000	15.8	21.0	Did not fail
18	121,900	20.0	26.9	Center

[a]Equivalent to maximum stresses from strain-gage data obtained on two specimens calibrated over the maximum test load range. Mean stress ranged from 12.5 to 13.0 ksi.

[b]Mean stress ranged from about 17.4 to 17.8 ksi.

TABLE VI

MECHANICAL PROPERTIES OF MATERIALS USED IN I-BEAMS[a]

Material	Tensile strength, ksi	Yield strength (0.2 percent offset), ksi	Elongation in 2 in., percent	Modulus of elasticity, psi
0.072-inch 2024-T3 aluminum-alloy sheet (sheet 1)	72.5	52.7	17.9	10.8×10^6
0.072-inch 2024-T3 aluminum-alloy sheet (sheet 2)	72.8	55.7	18.4	10.7
2024-T4 aluminum-alloy extruded angle	65.7	47.9	15.6	10.4

[a]Average strength values for four specimens.

TABLE VII

SUMMARY OF I-BEAM FATIGUE FAILURE DATA

Specimen	Failing member	Location of failure (a)	Fatigue life, cycles	Remarks
1	Chord	Between rivets 1 and 2	86,330	Failure associated with metallographic flaw on surface
1-1	2 chords	Rivet 3	137,800	Catastrophic failure
2	2 chords	Rivet 3	75,350	
2-1	1 chord 1 web	Rivet 3	1,915,480	Failures associated with same rivet hole

[a]See figure 18.

TABLE VIII

STRESSES IN I-BEAMS

Specimen	Bending moment Pa, 1,000 in-lb		Fatigue life, cycles	Measured chord stress, ksi		Calculated chord stress, ksi (b)			
						Based on gross area		Based on net area	
	Maximum	Mean	(a)	Maximum	Mean	Maximum	Mean	Maximum	Mean
1	253	133	86,330	23.0	11.9	26.6	14.0	-----	---
1-1	249	128	137,800	15.0	7.8	17.0	8.7	17.2	8.9
2	256	135	75,350	15.8	8.2	17.5	9.2	17.8	9.4
2-1	176	118	1,915,480	12.0	8.0	12.0	8.1	12.2	8.2

[a]See table VII and figure 18 for location of failure.

[b]Calculations based on moment of inertia at cross section associated with failure.

TABLE IX

RESULTS OF FATIGUE TESTS ON SIMULATION COUPONS, TYPE D, FOR I-BEAM

Specimen	Computed stresses, ksi (a)	Loading stresses from strain gages, ksi (b)	Lifetime to failure
1	11.5 ± 10.8	9.9 ± 8.3	468,000
2	10.8 ± 9.7	10.9 ± 6.8	628,000
3	10.8 ± 9.7	9.3 ± 7.1	738,000
[c]4	11.5 ± 8.4	7.8 ± 6.8	136,000
5	8.4 ± 8.3	7.3 ± 5.1	3,222,000
6	8.3 ± 6.4	6.0 ± 4.5	2,507,000
[c]7	13.0 ± 6.4	9.8 ± 1.0	1,235,000

[a]Computed stresses at rivet center line were obtained from $S = \frac{P}{A} + \frac{My}{I}$, where P is either mean or alternating load and $M = \frac{Pe}{6}$; $\frac{P}{6}$ is used on the assumption that the first five rivets of the group of six rivets take altogether 5/6 P. In this expression e and y represent distance between center line of chord and rivet row.

[b]See text for method of extrapolation.

[c]Indication, from other gages, of unusual gradient.

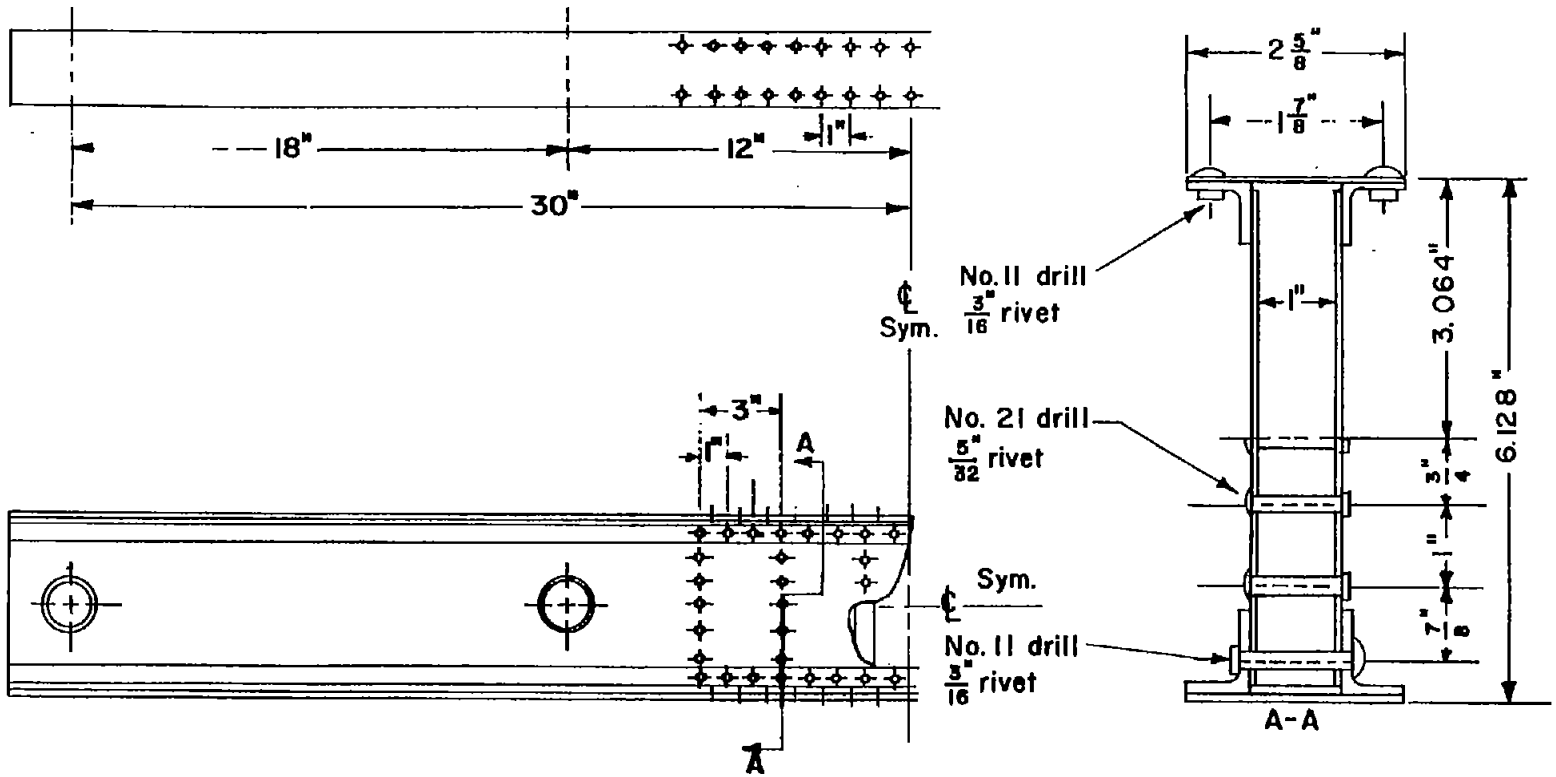

Figure 1.- Schematic drawing of box-beam specimen. For section A-A: top skin, 0.064-inch sheet; bottom skin, 0.064-inch sheet; webs, 0.051-inch sheet; chord angles, 0.75 × 0.75 × 0.091-inch extrusion; stiffeners, 1 × $\frac{5}{8}$-inch block; moment of inertia (based on net area), 7.75 inch^4; and moment of inertia (based on gross area), 8.73 inch^4.

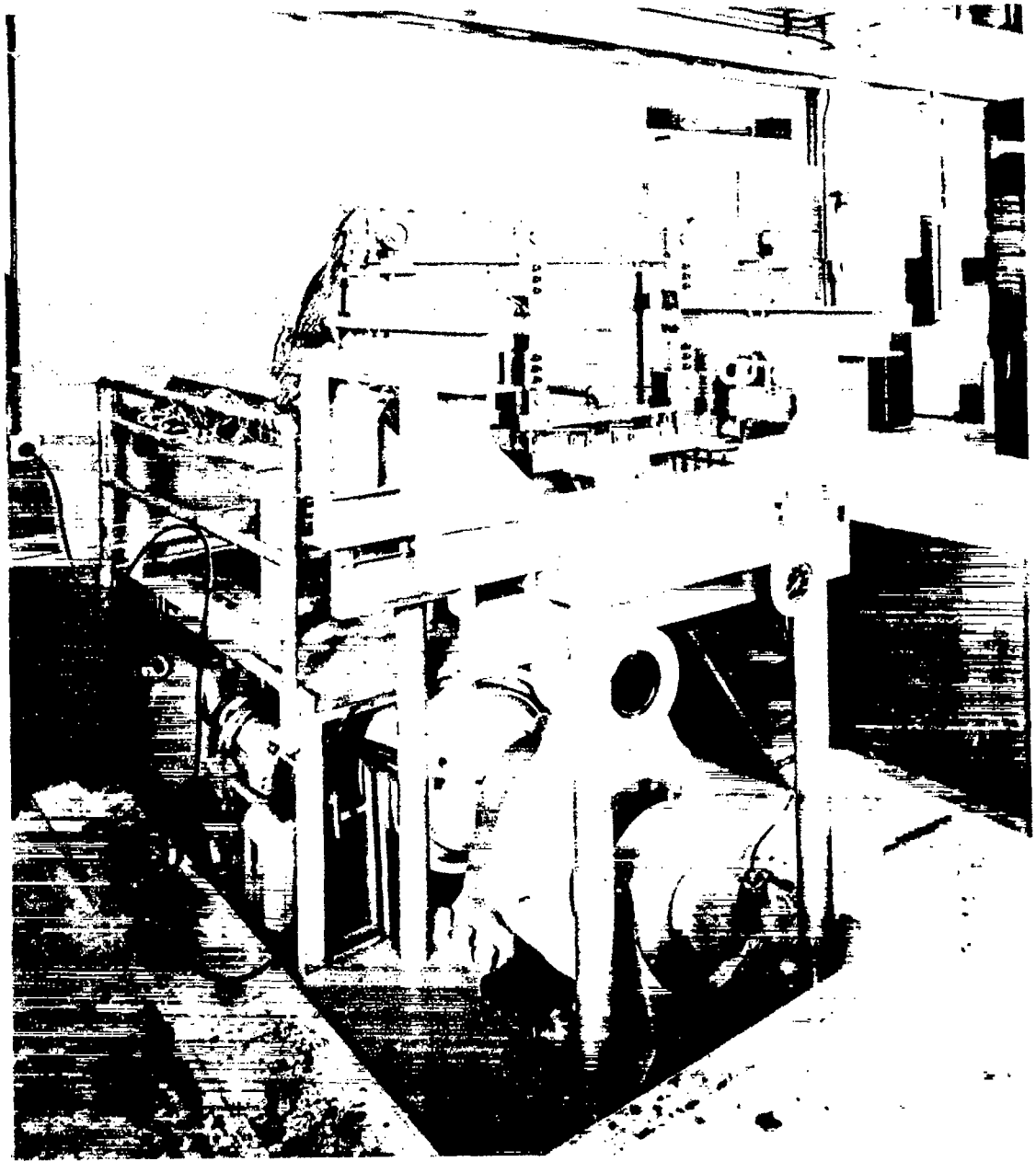

L-57-3623

Figure 2.- Test setup for static and fatigue testing of box-beam specimen.

L-57-3624

Figure 3.- Closeup view of box-beam and loading fixture.

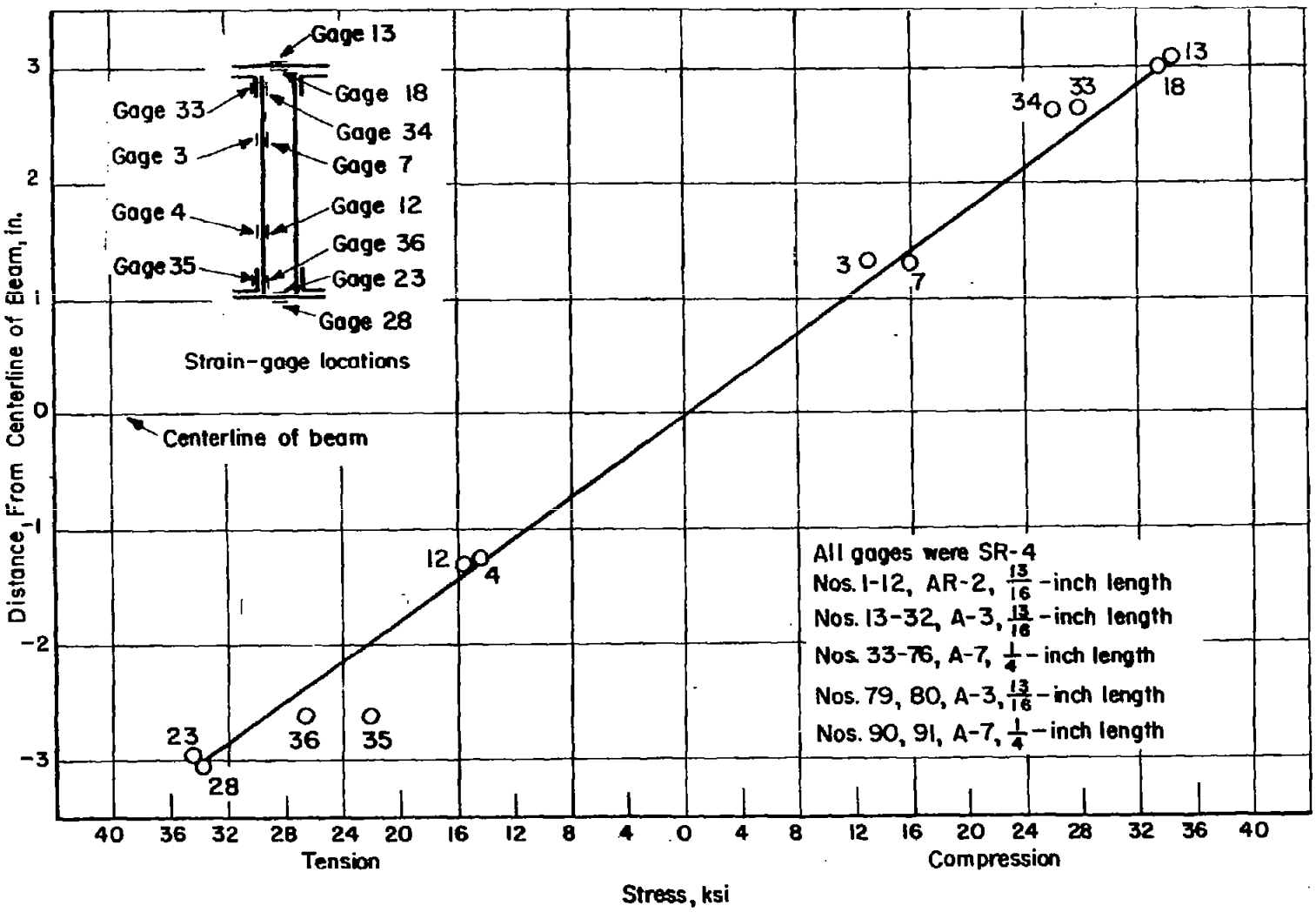

Figure 4.- Stress distribution on section D-D for 90,000 inch-pound bending moment. For strain-gage locations see section D-D in figure 8.

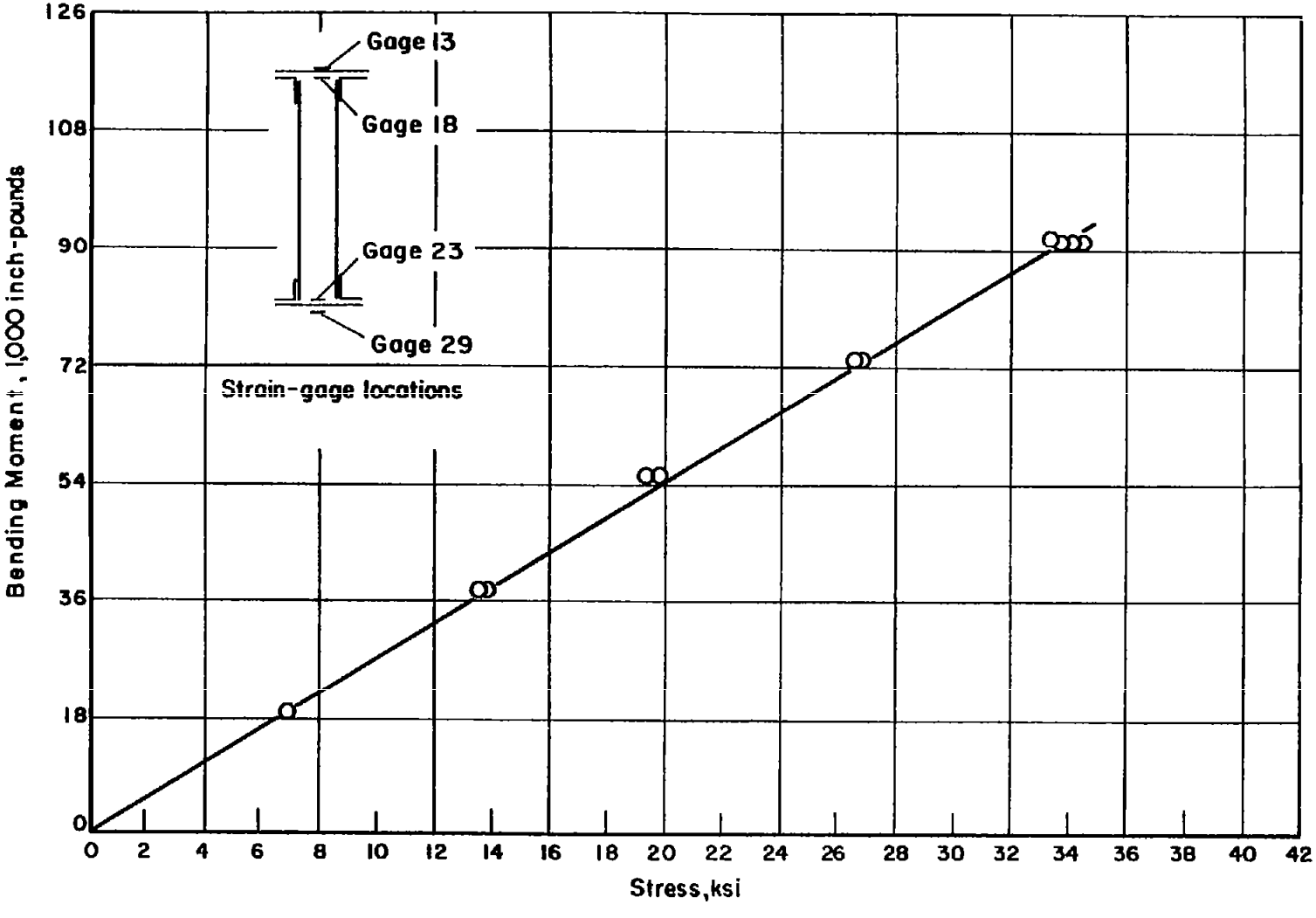

Figure 5.- Stress variation of skin of section D-D with applied moment. For strain-gage locations see section D-D in figure 8.

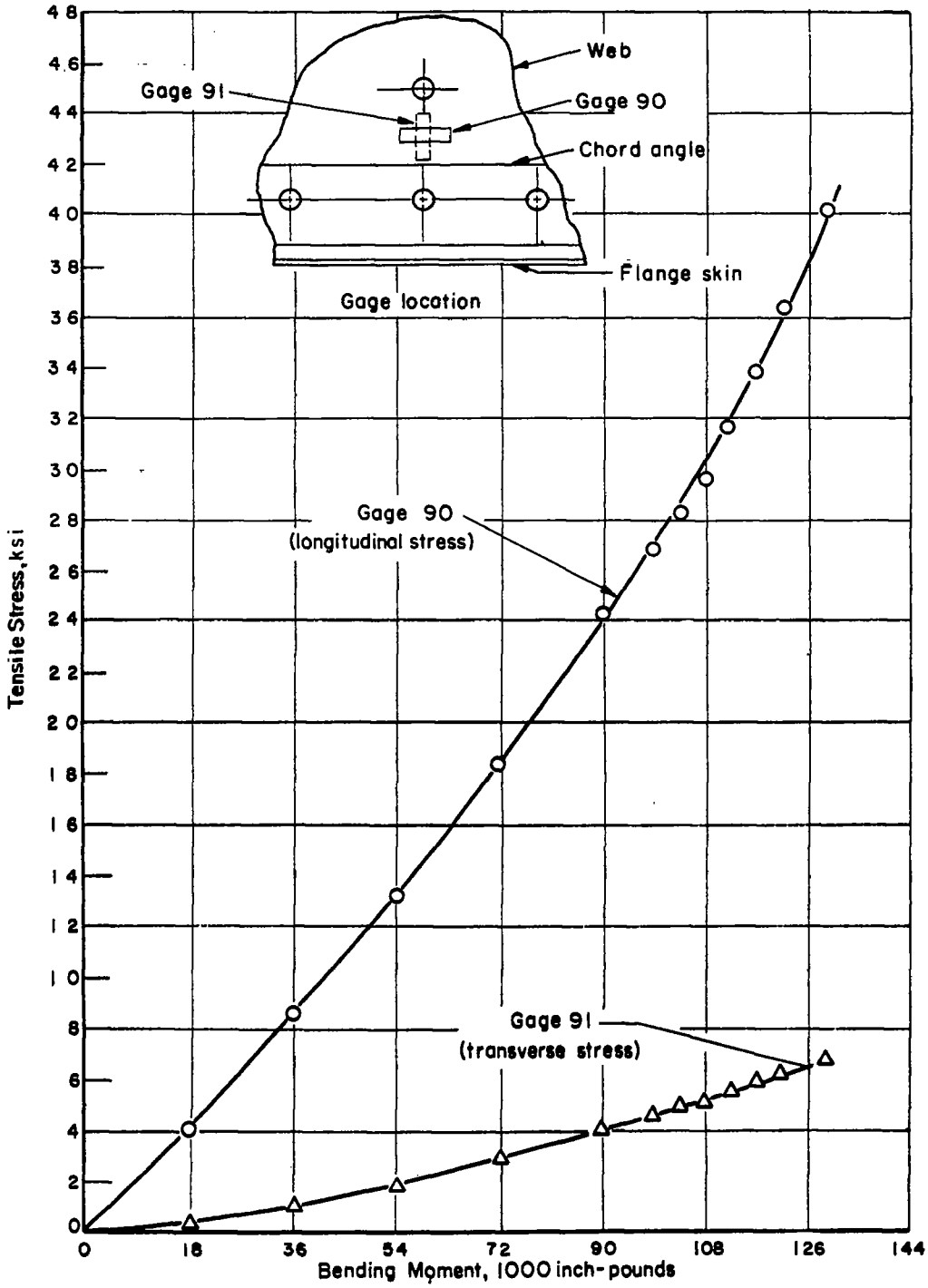

Figure 6.- Stress variation of box-beam web (between stiffener rivets) with variation in bending moment.

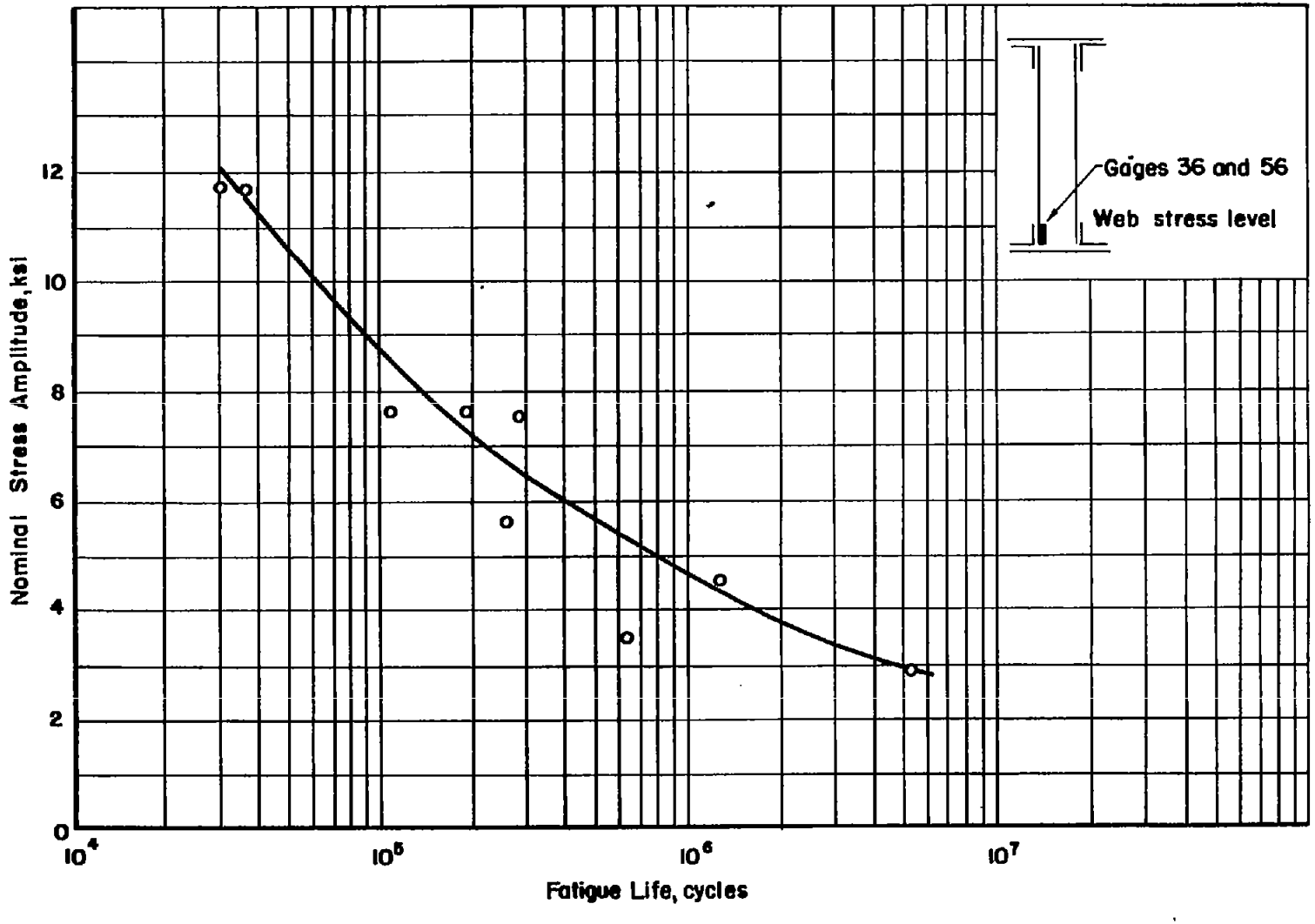

Figure 7.- Results of bending fatigue tests on box-beam web section at 12.5-ksi mean stress.

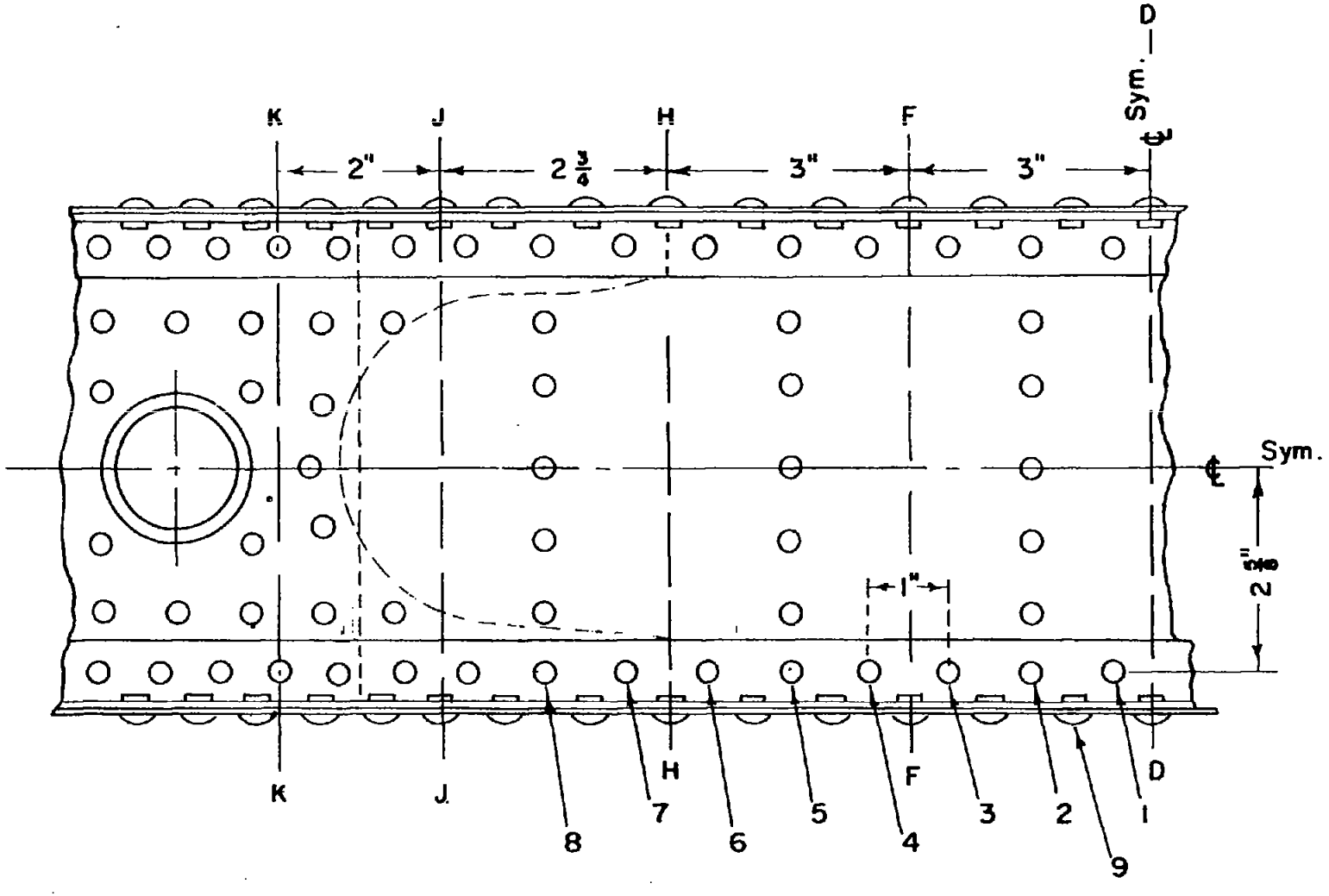

Figure 8.- Box-beam specimen, midspan-rivet pattern. Numbers indicate locations of failure in box beam.

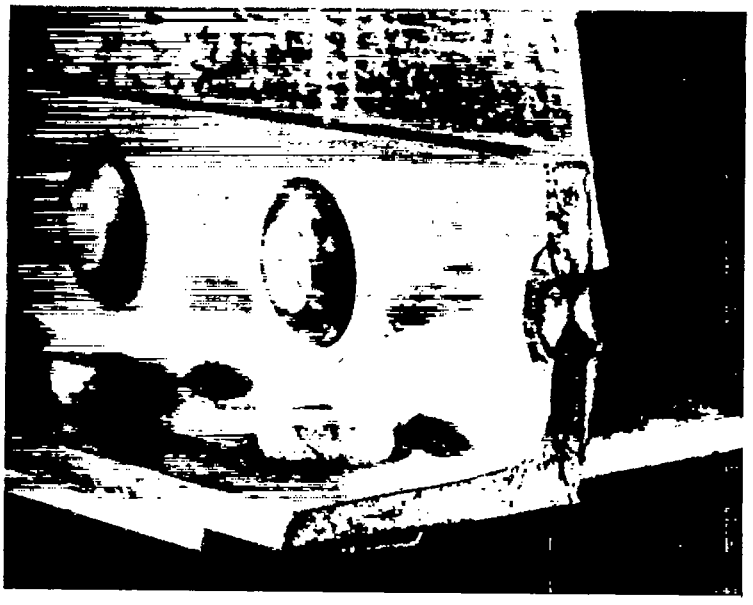

L-57-3625

Figure 9.- Fractured surface at fatigue nuclei of box-beam 2.

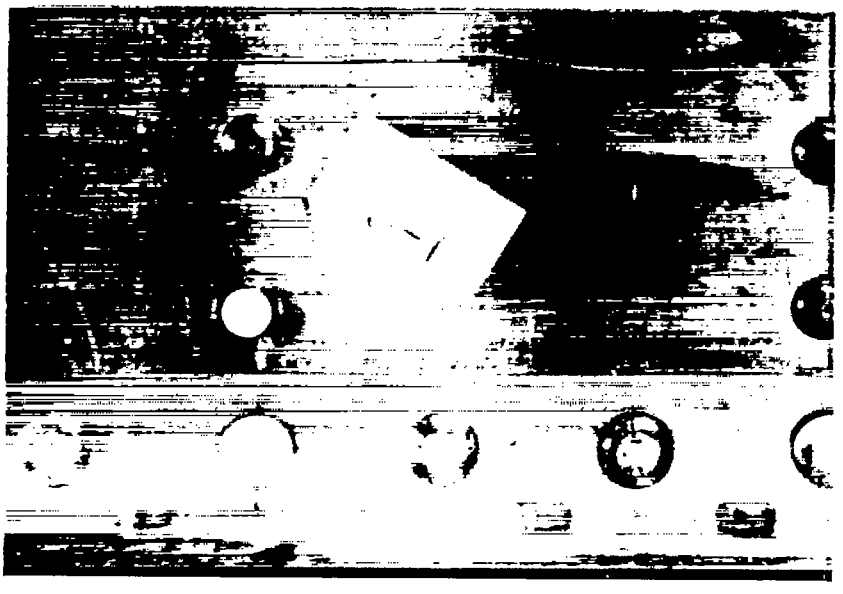

L-57-3626

Figure 10.- Fatigue crack in box-beam 6-1.

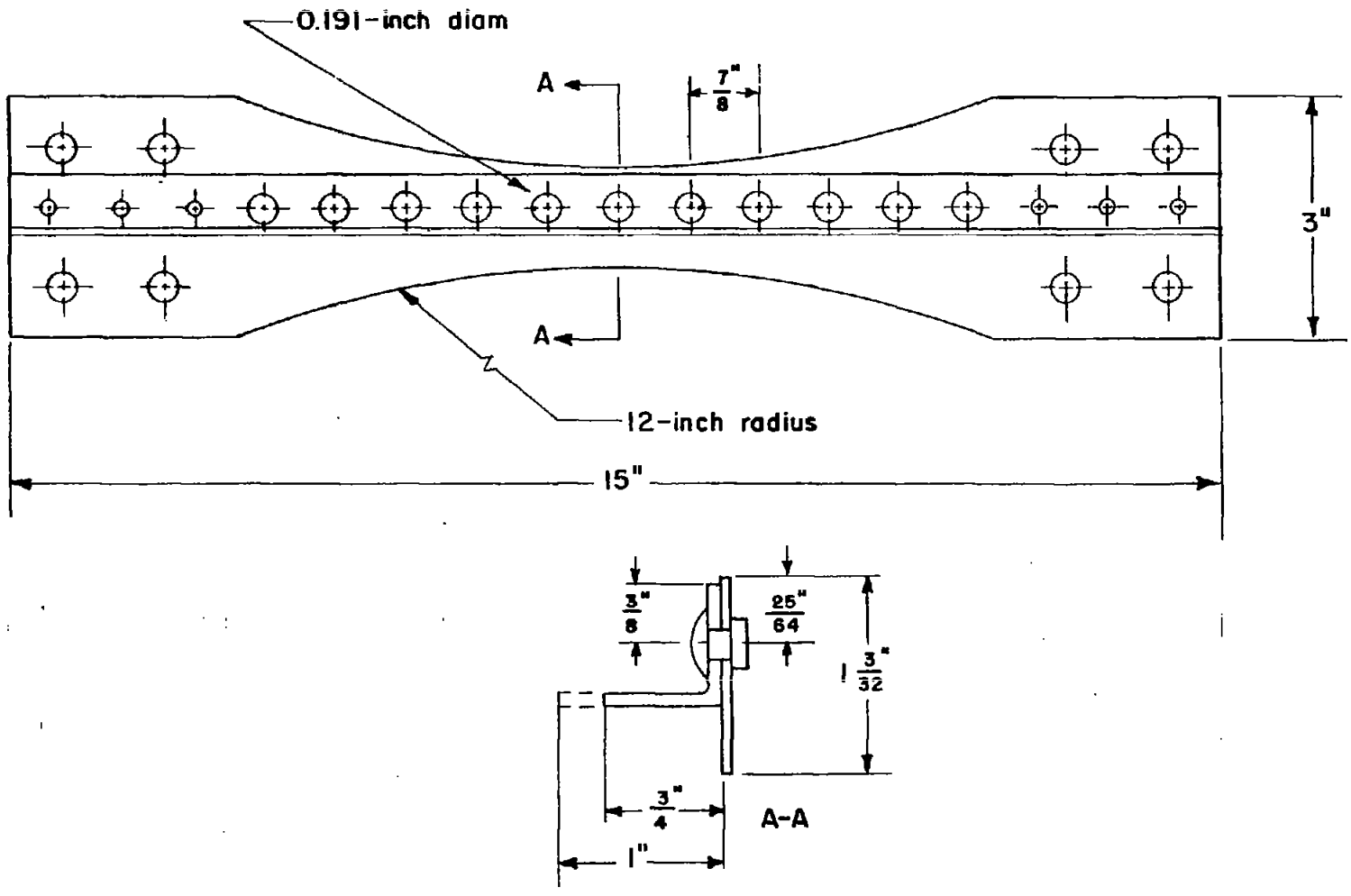

Figure 11.- Detailed drawing of the first simulation element. For section A-A: web, 0.051-inch sheet; chord angle, 0.75 x 0.75 x 0.091-inch extrusion; and rivets, $\frac{3}{16}$-inch diameter.

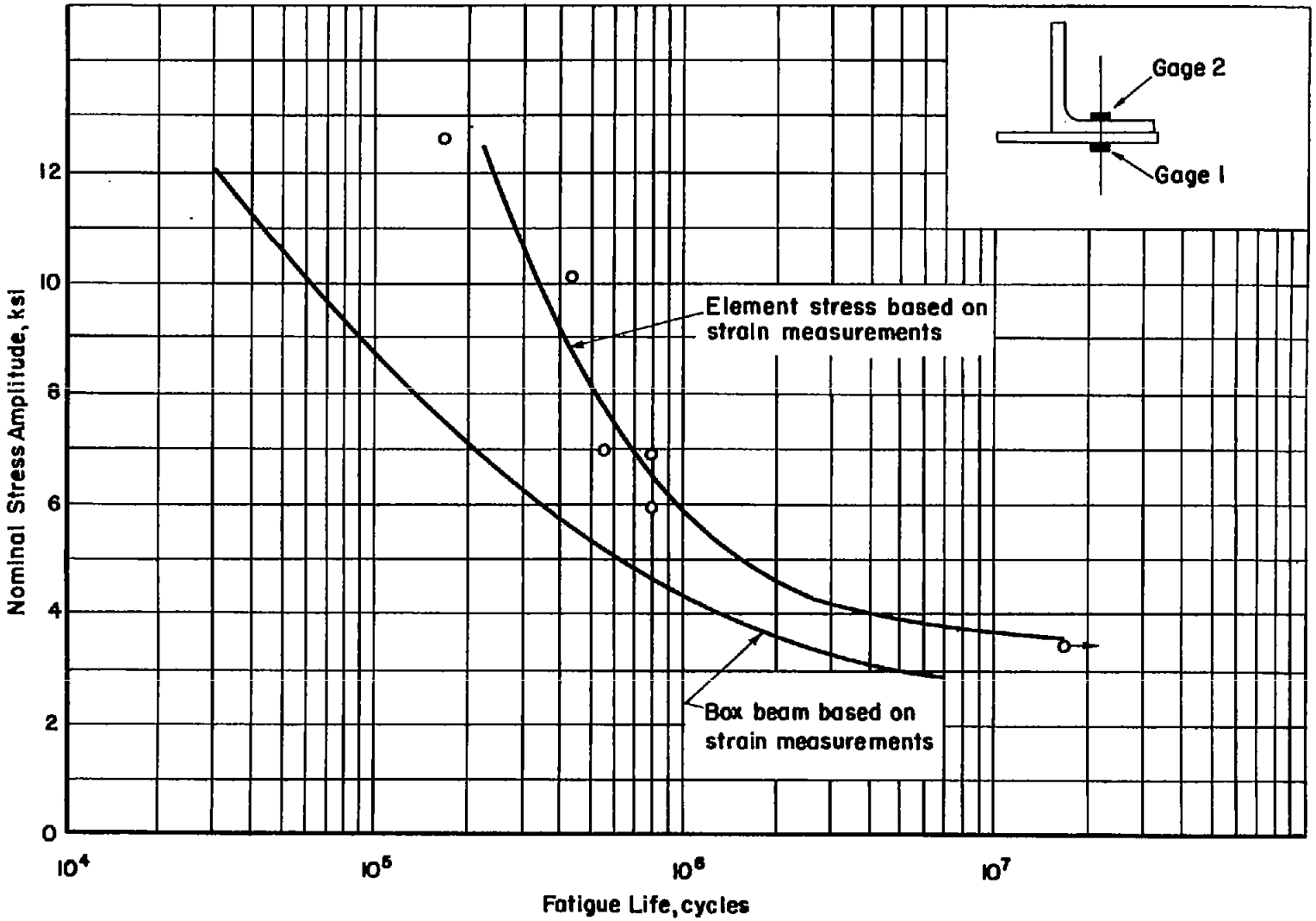

Figure 12.- Results of axial-load fatigue tests on the first simulation element for box beam. Mean stress, 12.5 ksi.

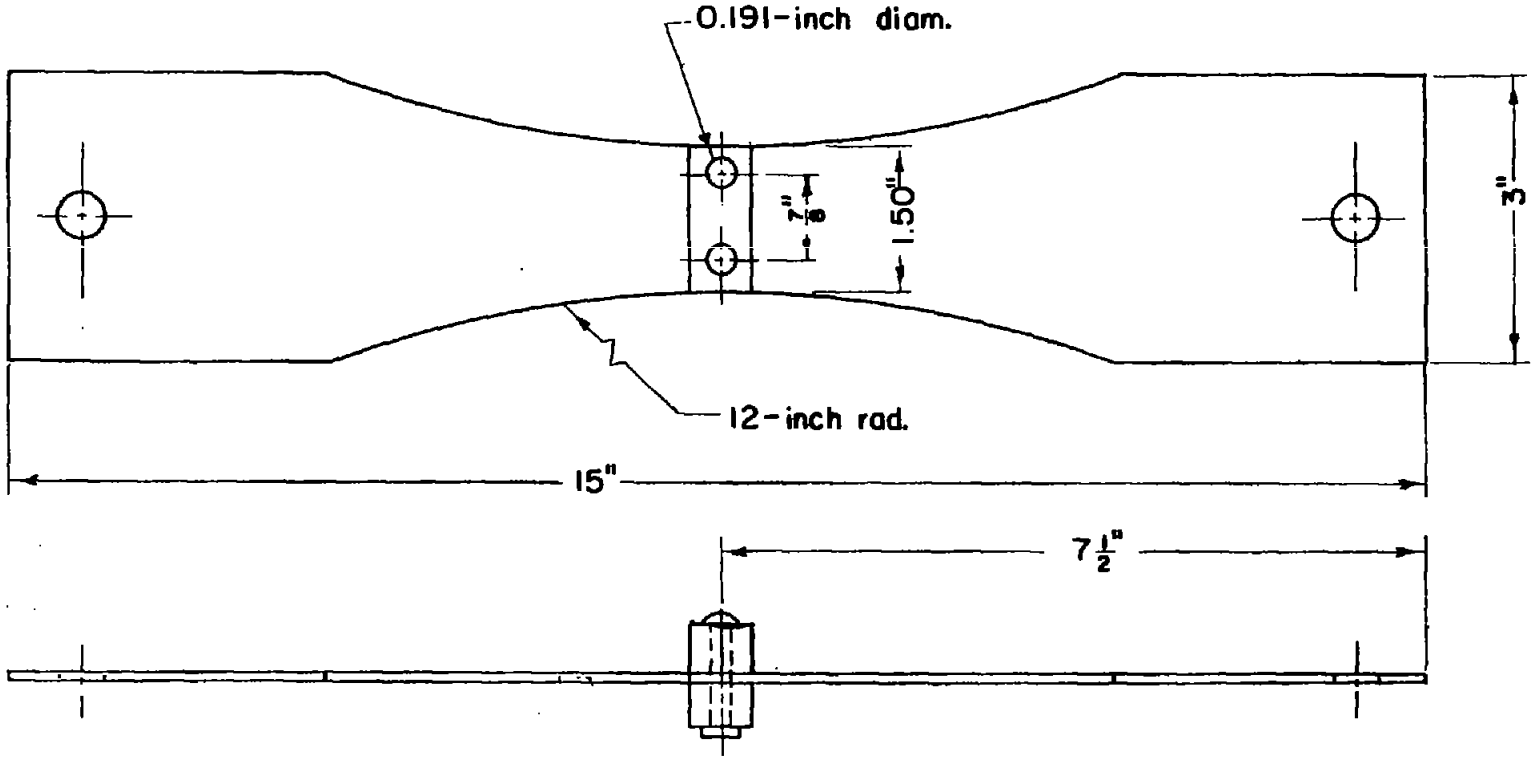

Figure 13.- Detailed drawing of second simulation element. Web, 0.051-inch sheet; stiffeners, $\frac{1}{2}$- x $\frac{5}{8}$- inch extrusion; and rivets, $\frac{3}{16}$- inch diameter.

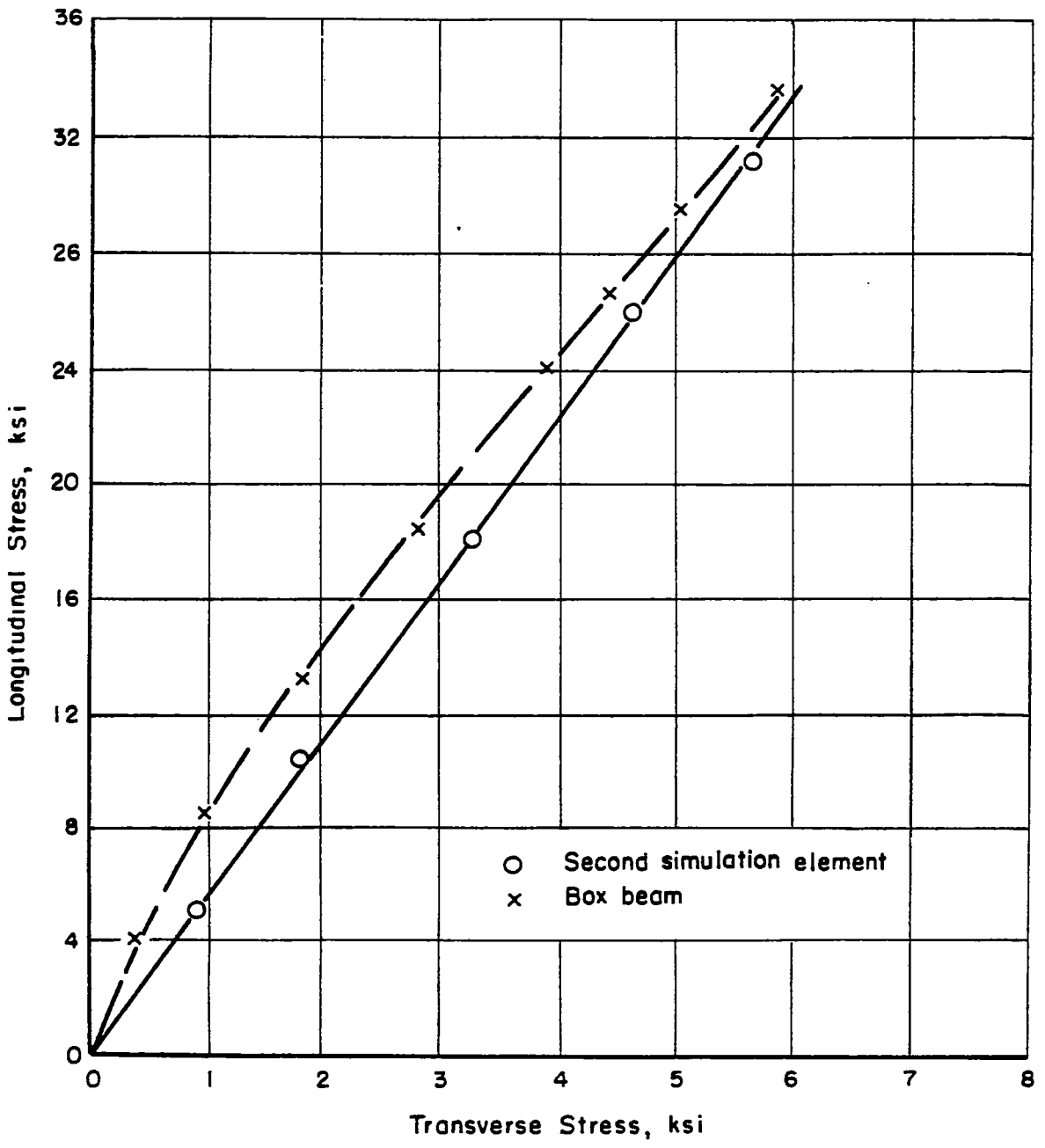

Figure 14.- Comparison of longitudinal-stress—transverse-stress relationship of second simulation element and box beam.

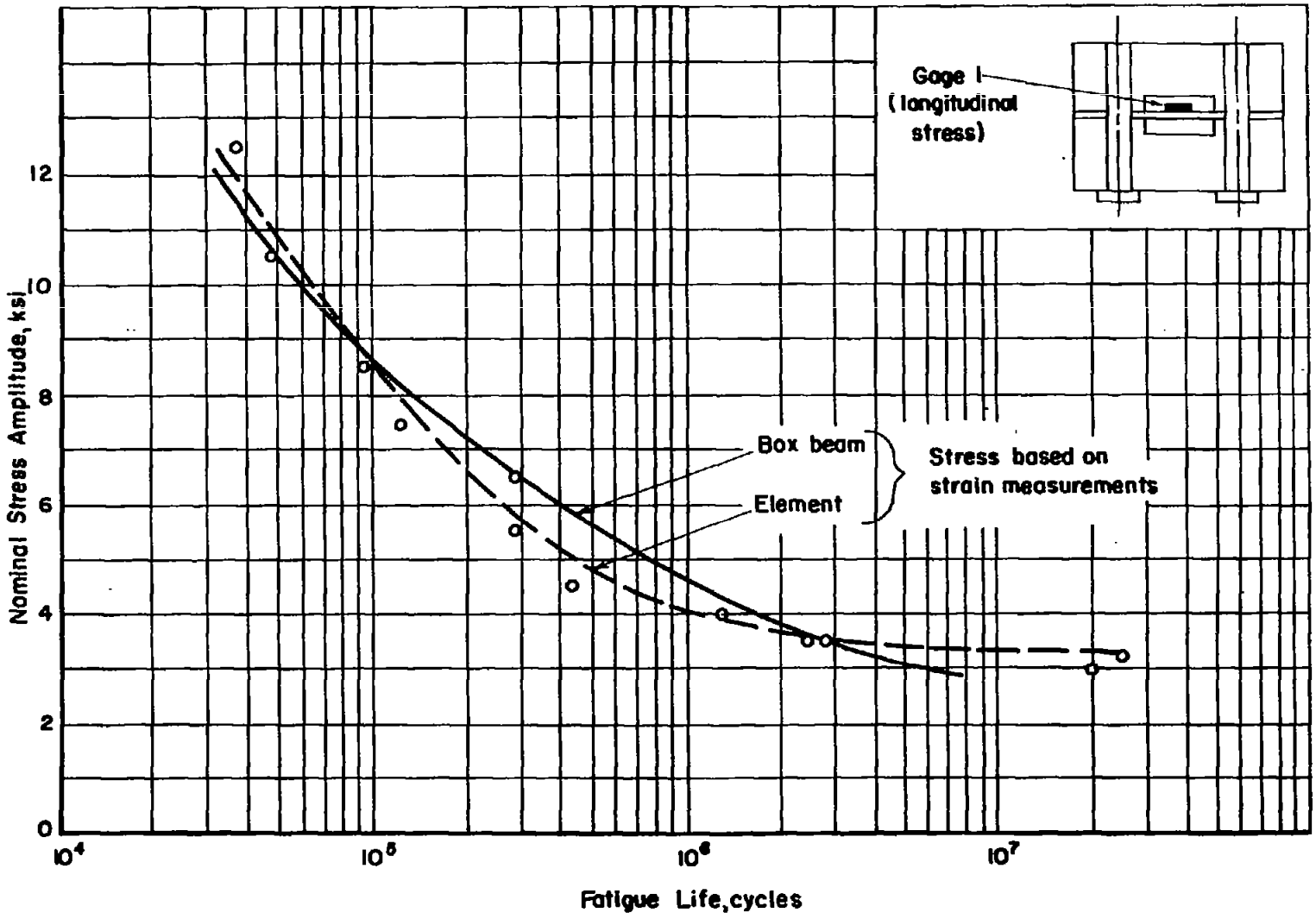

Figure 15.- Results of axial-load fatigue tests on second simulation element for box beam.

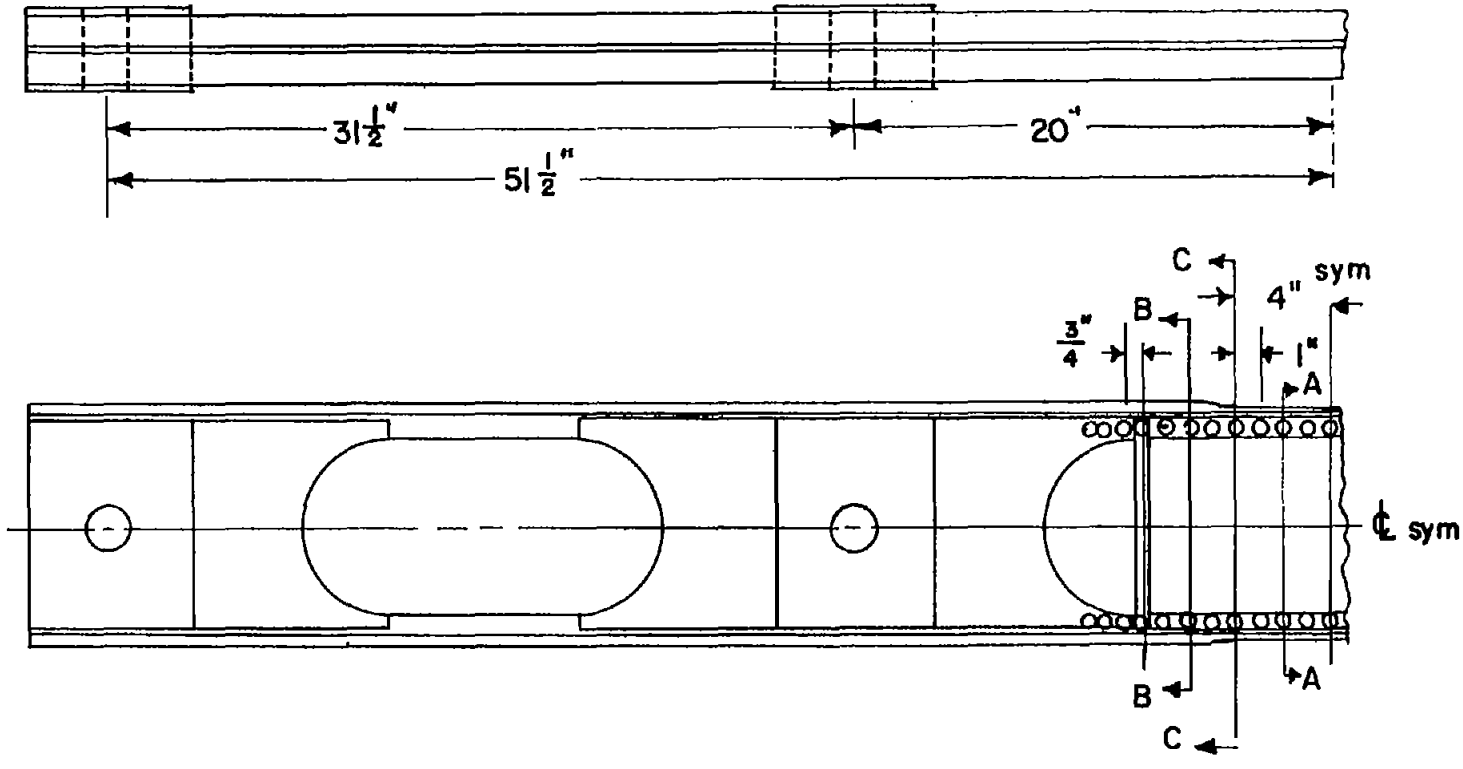

Figure 16.- Schematic drawing of I-beam specimen.

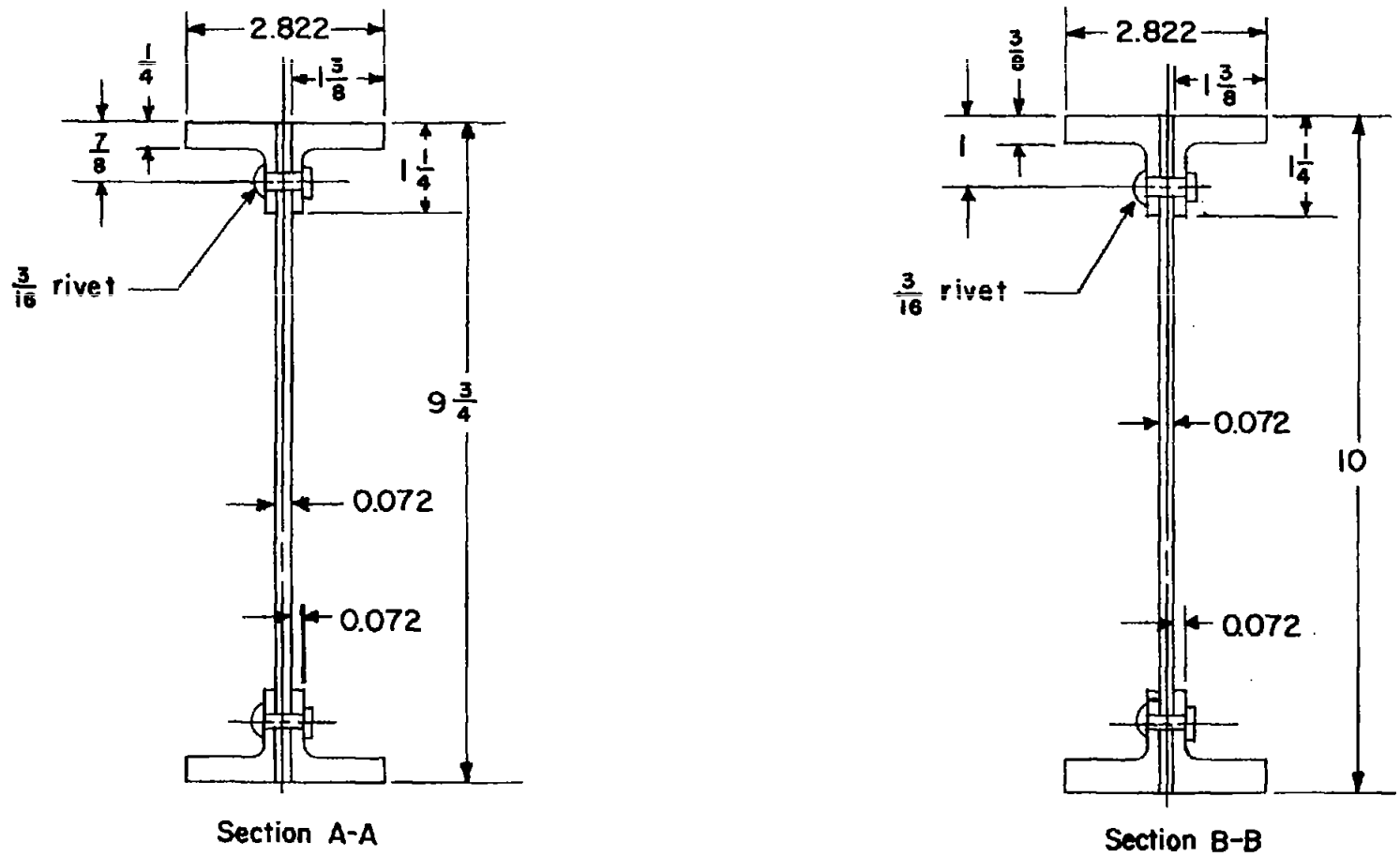

Figure 17.- Beam sections of specimen shown in figure 16. For section A-A, I_{XX} = 40.88 inches^4 and I_{gg} = 41.55 inches^4; for section B-B, I_{XX} = 57.8 inches^4 and I_{gg} = 58.7 inches^4.

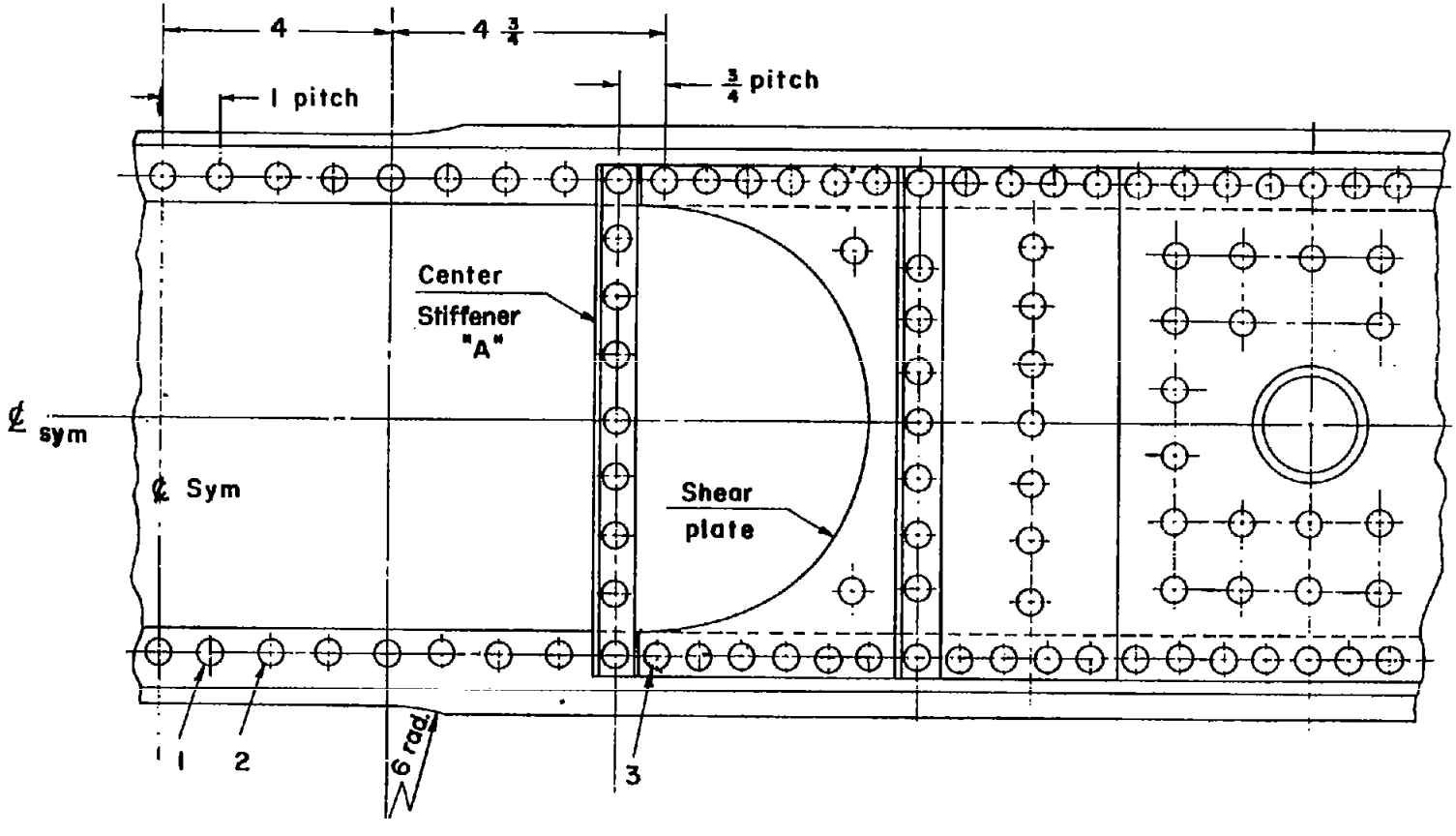

Figure 18.- I-beam specimen, midspan-rivet pattern.

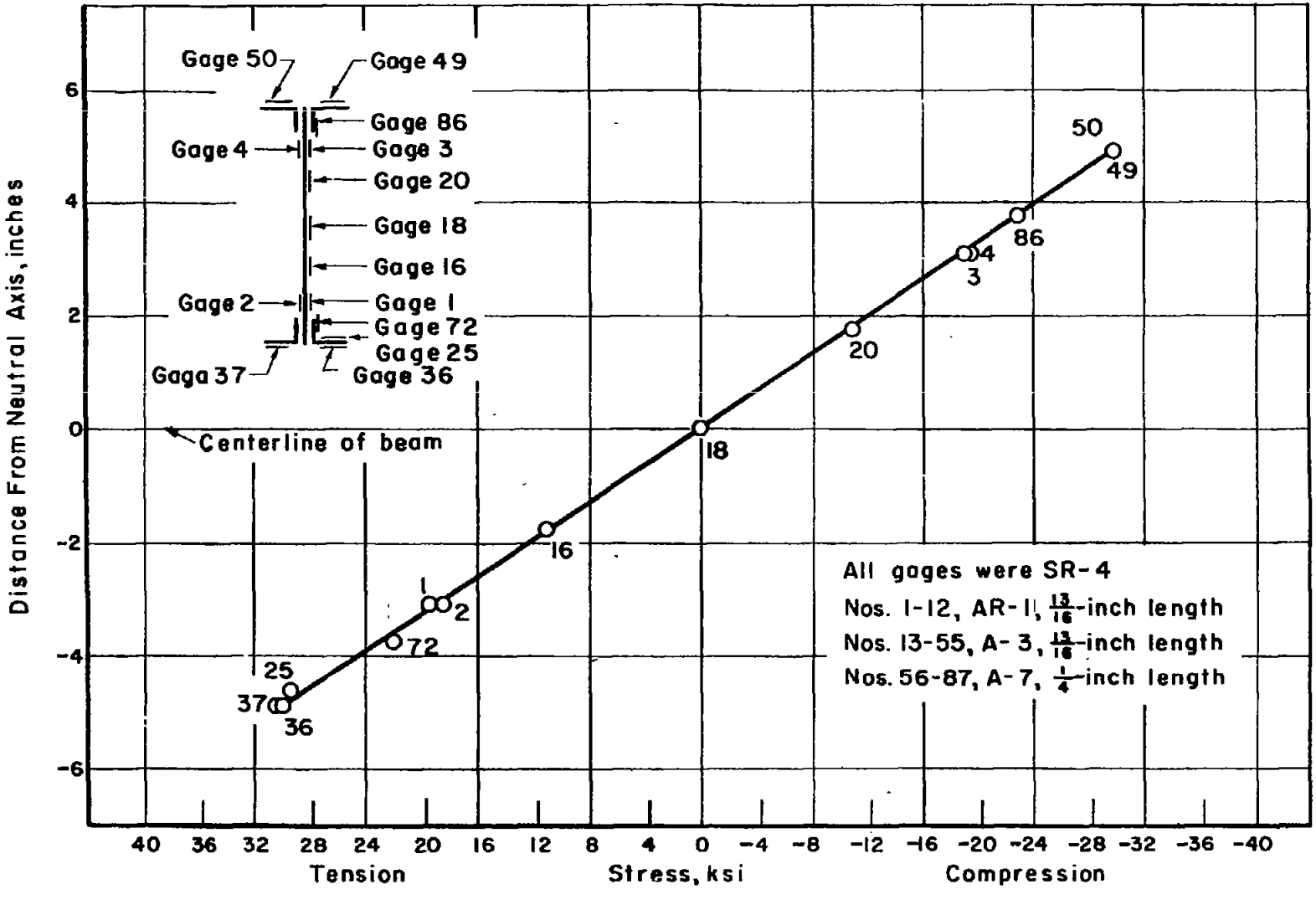

Figure 19.- Stress distribution on cross section at center of midspan of I-beam for 270,000 inch-pound bending moment.

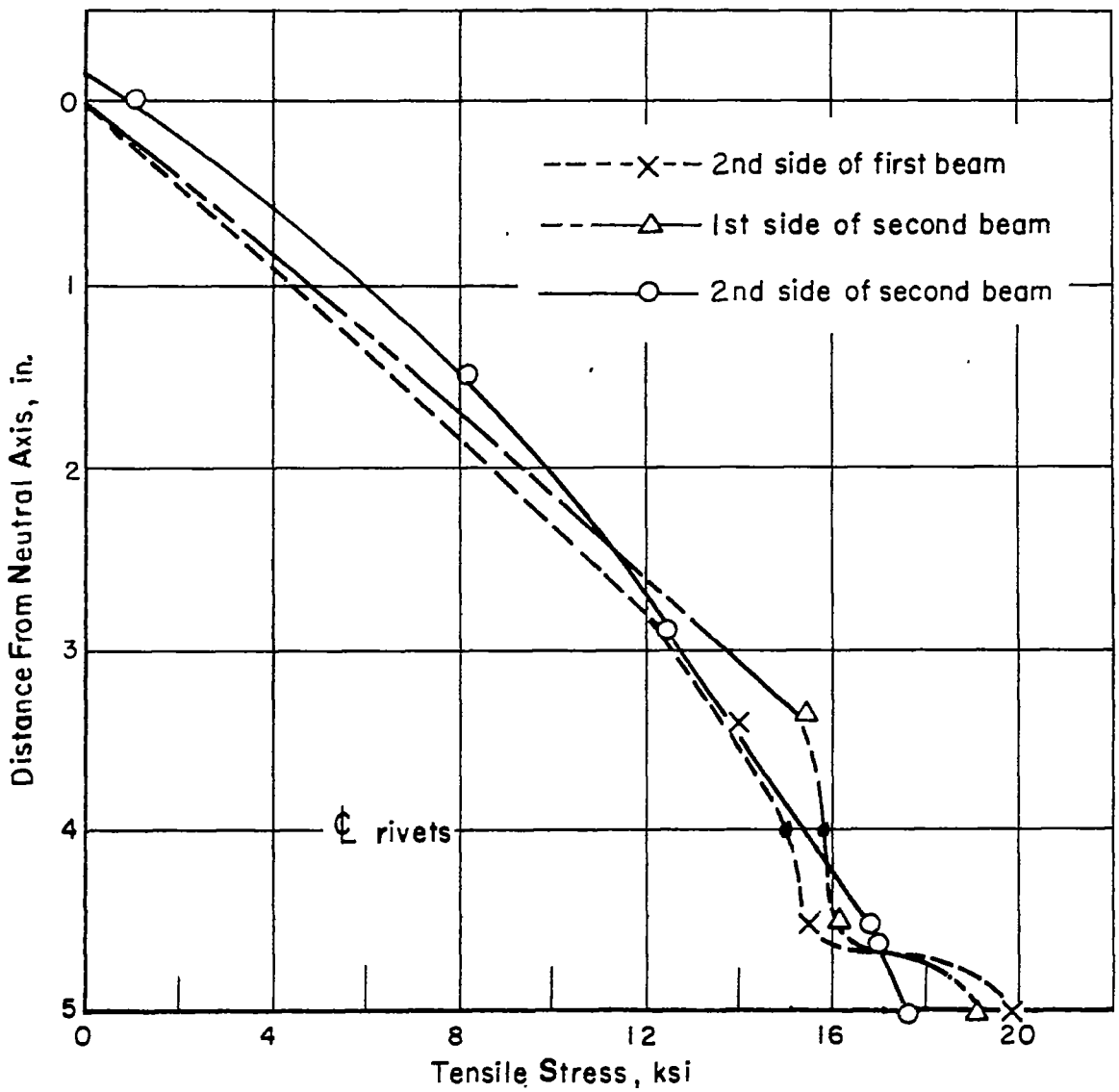

Figure 20.- Tensile-stress distribution at cross section through first rivet in shear plate of I-beam for applied bending moment of 240,000 inch-pounds.

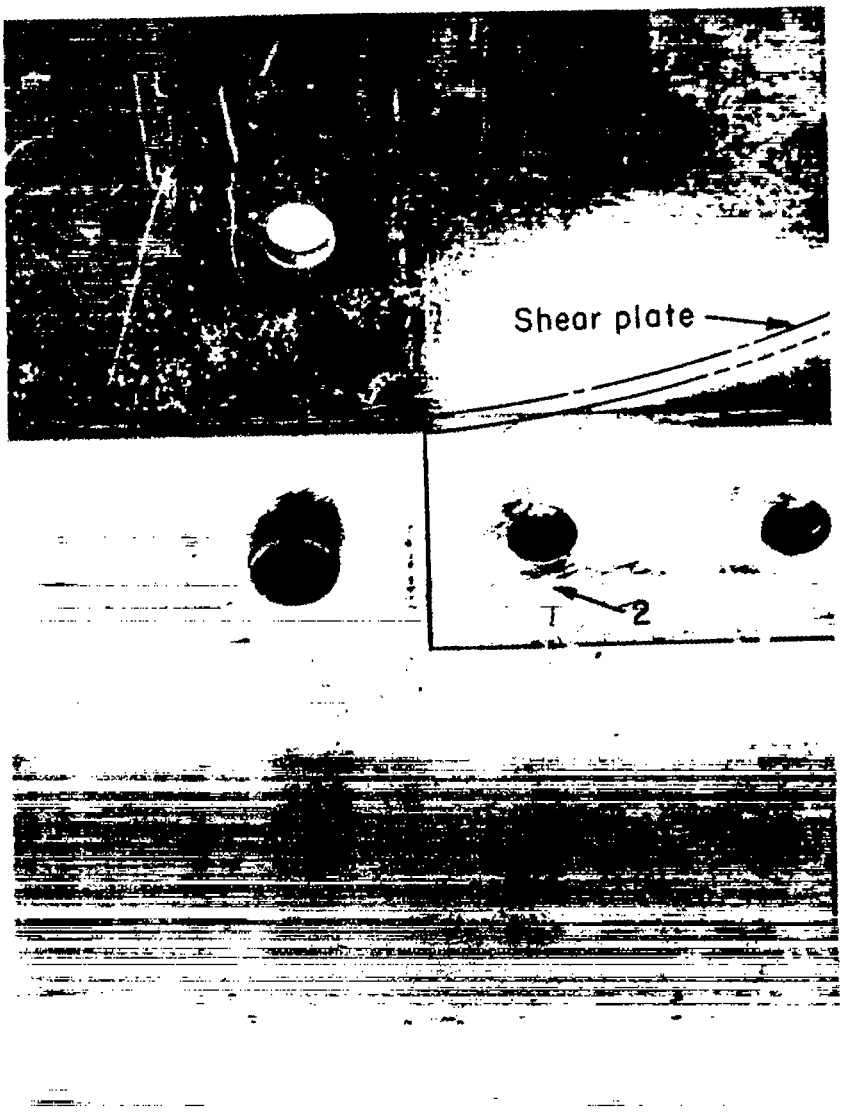

L-57-3627

Figure 21.- Fatigue failure in second I-beam.

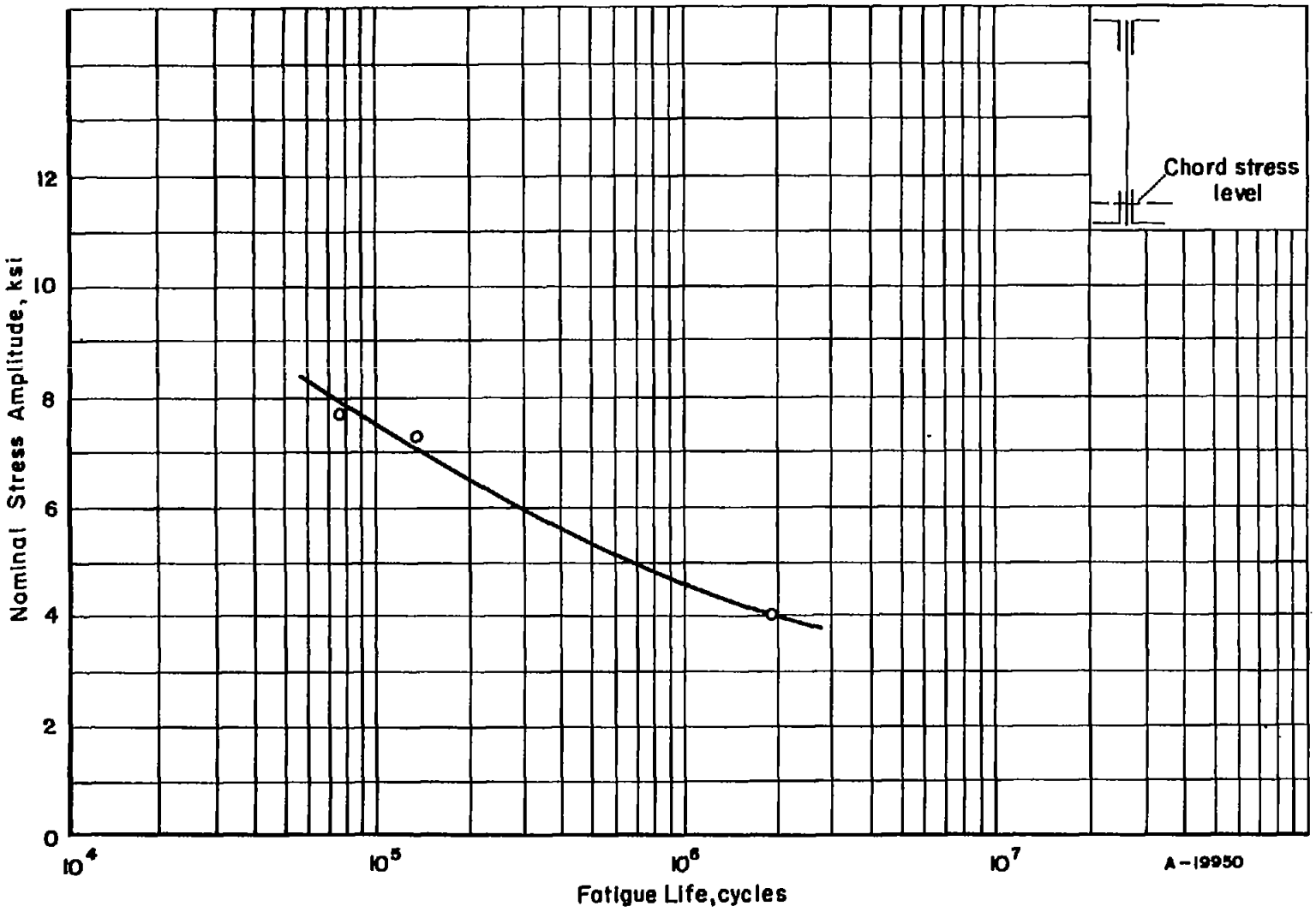

Figure 22.- Results of bending fatigue tests on I-beam chord section at 8-ksi measured mean stress.

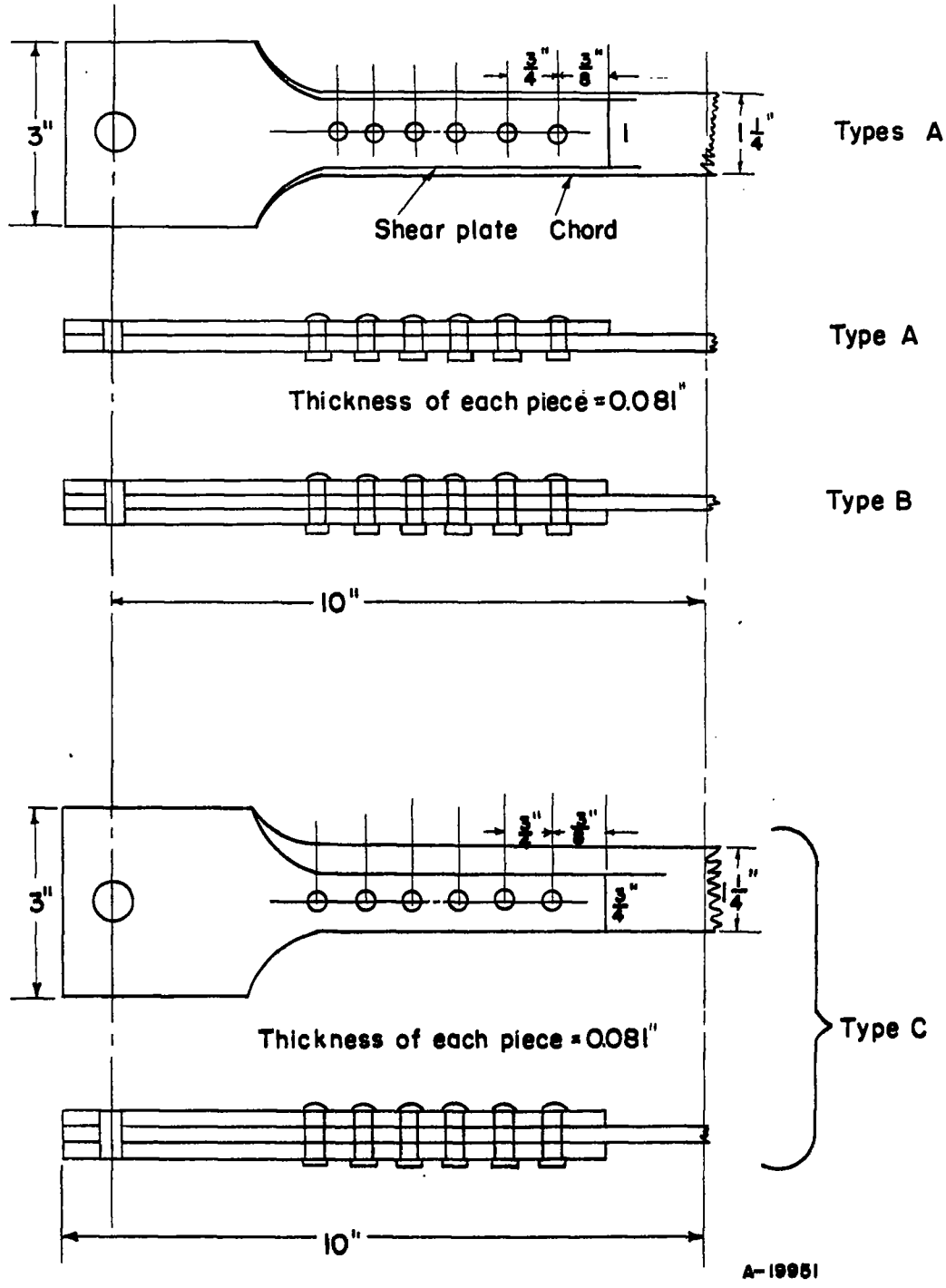

Figure 23.- Elements in preliminary tests for simulation of I-beam.

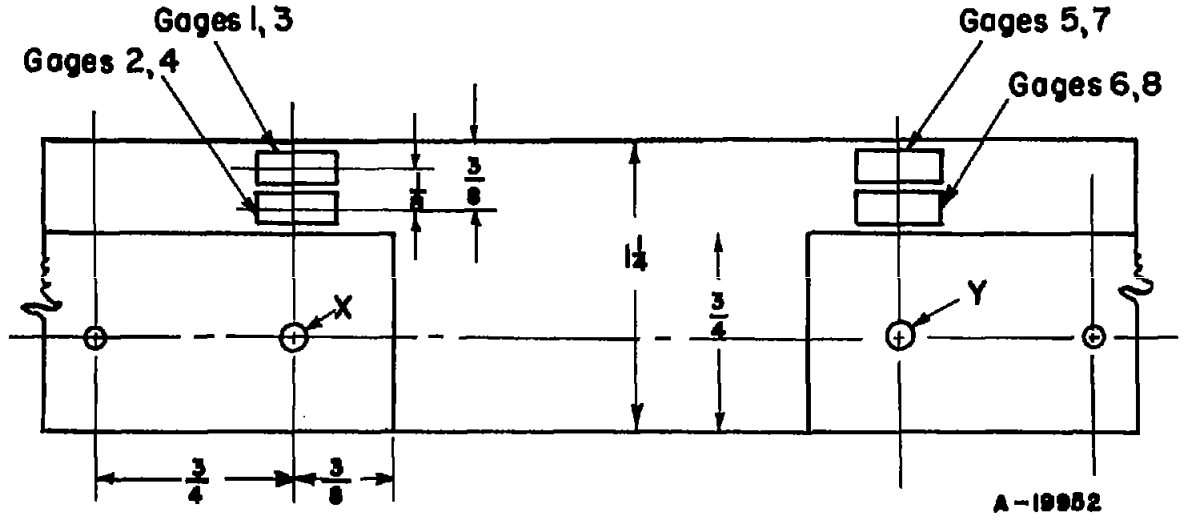

Gages 1, 2, 5, 6 on front side
Gages 3, 4, 7, 8 on reverse side

Figure 24.- I-beam element (type D) with location of eight strain gages indicated.

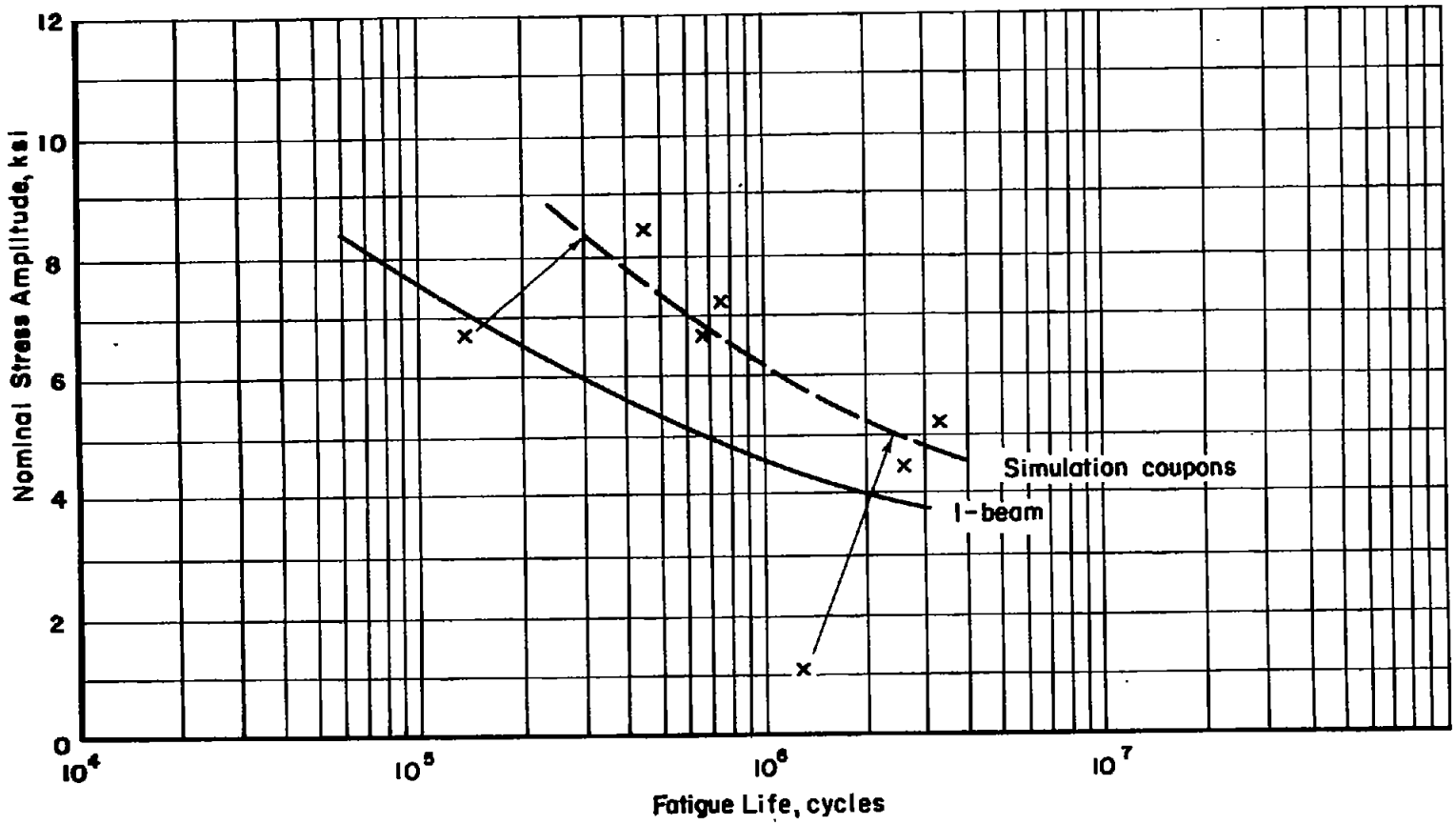

Figure 25.- Results of fatigue tests on simulation elements for I-beam.

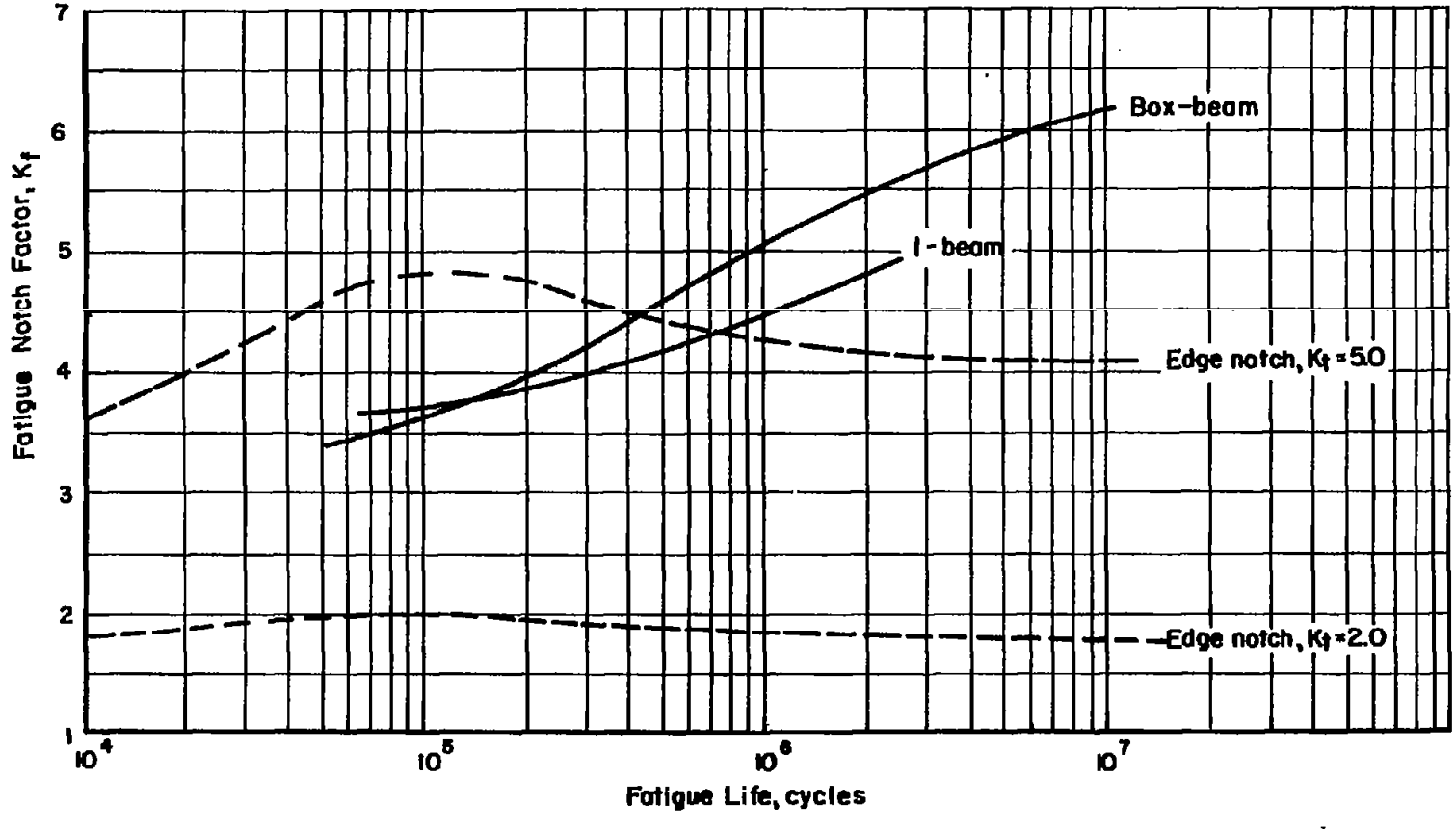

Figure 26.- Fatigue notch factors in beam tests.

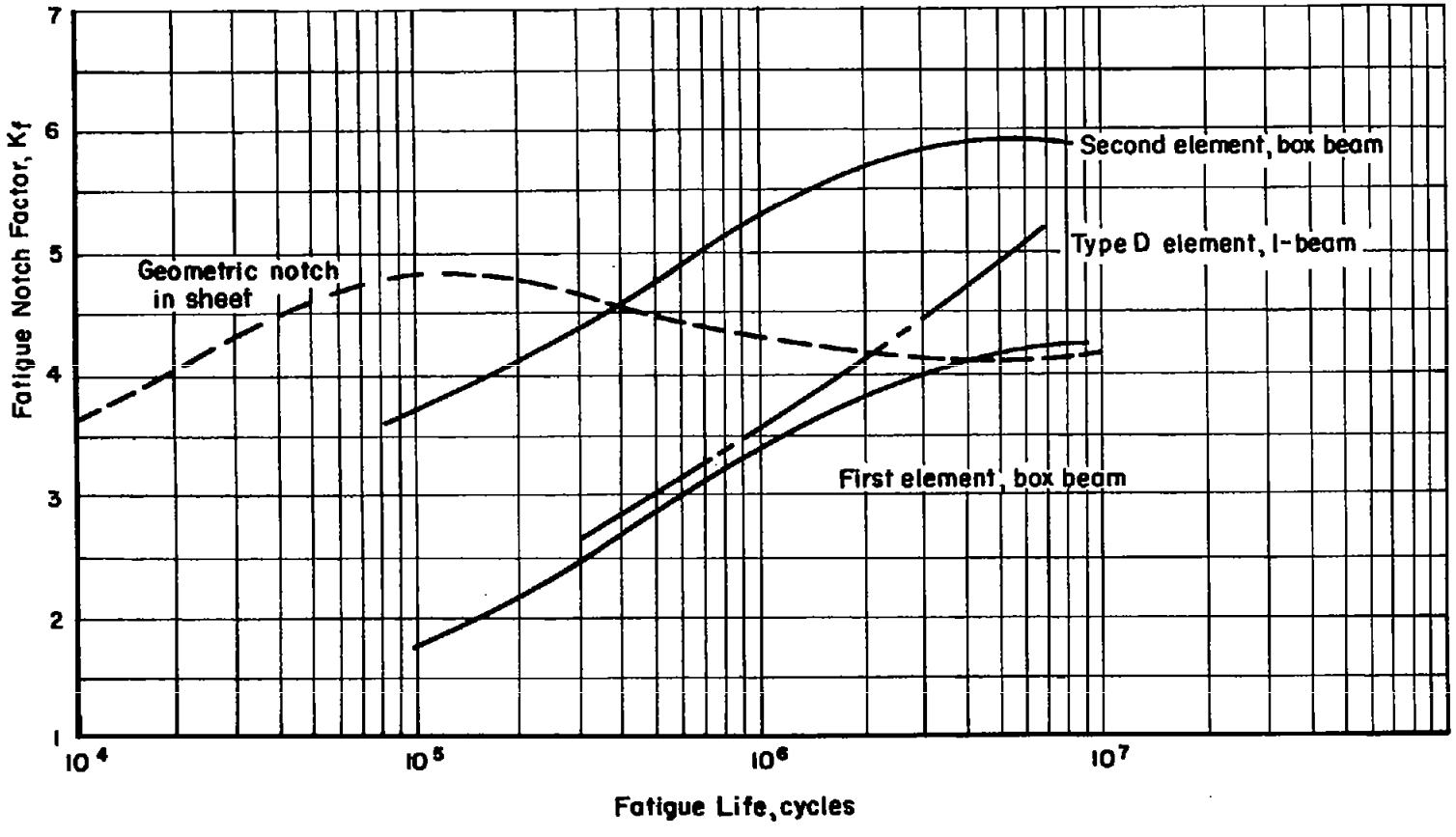

Figure 27.- Fatigue notch factors for simulation elements.

NACA - Langley Field, Va.